MARMARA UNIVERSITY
INSTITUTE FOR GRADUATE STUDIES
IN PURE AND APPLIED SCIENCES

PHOSPHATE RECOVERY FROM SEWAGE SLUDGE SUPERNATANTS USING MAGNETIC NANOPARTICLES

ANETT GULYÁS

MASTER THESIS
Department of Environmental Sciences

ThesisSupervisor
Doç. Dr. Neslihan SEMERCI

ISTANBUL, 2019

MARMARA UNIVERSITY
INSTITUTE FOR GRADUATE STUDIES
IN PURE AND APPLIED SCIENCES

PHOSPHATE RECOVERY FROM SEWAGE SLUDGE SUPERNATANTS USING MAGNETIC NANOPARTICLES

ANETT GULYÁS
(526116921)

MASTER THESIS
Department of Environmental Sciences

ThesisSupervisor
Doç. Dr. Neslihan SEMERCI

ISTANBUL, 2019

MARMARA UNIVERSITY
INSTITUTE FOR GRADUATE STUDIES IN PURE AND APPLIED SCIENCES

Anett GULYÁS, a Master of Science student of Marmara University Institute for Graduate Studies in Pure and Applied Sciences, defended her thesis entitled "**Phosphate recovery from sewage sludge supernatants using magnetic nanoparticles**", on November 27, 2019 and has been found to be satisfactory by the jury members.

Jury Members

Doç. Dr. Neslihan SEMERCI (Advisor)
Marmara University ..... (SIGN) .....

Prof. Dr. Zehra Semra CAN (Jury Member)
Marmara University ..... (SIGN) .....

Prof. Dr. Nihal BEKTAŞ (Jury Member)
Gebze Technical University ..... (SIGN) .....

APPROVAL

Marmara University Institute for Graduate Studies in Pure and Applied Sciences Executive Committee approves that Anett GULYÁS be granted the degree of Master of Science in Department of Environmental Sciences, Environmental Sciences Program on November 27, 2019. (Resolution no: 2019/24-02

Director of the Institute
Prof. Dr. Bülent EKİCİ

ACKNOWLEDGEMENT

Firstly, I would like to express my appreciation to my thesis supervisor, Doç. Dr. Neslihan SEMERCI, who showed me an interesting, new and rarely known topic. I am thankful for her to guide and support me, moreover share her knowledge.

I would like to thank to the members of thesis committee, Prof. Dr. Zehra Semra CAN and Prof. Dr. Nihal BEKTAŞ for their valuable contributions.

I would like to express my thanks to Dr. Öğr. Üyesi Seval GENÇ to help in the production and characterization of magnetic nanoparticles. I am thankful to Öğr. Gör. Fatih Serdar SAYIN for FT-IR, EDX and SEM analysis, and to Prof. Dr. Sinan KESKIN for XRD. Also I would like to thank to Prof. Dr. Zehra Semra CAN, Dr. Arş. Grv. Gül Gülenay HACIOSMANOĞLU, Sevil COŞGUN and the other helpful member of Marmara University Engineering Faculty's laboratory for their assist, help, encouragement and suggestion especially during our laboratory studies.

I would like to acknowledge the financial support provided by Marmara University through BAPKO project: FEN-C-YLP-100719-0251.

I would like to thank to my scholarship giver, YTB (Yurtdışı Türkler ve Akraba Topluluklar Başkanlığı), for giving me the opportunity to study in Istanbul, Turkey.

Last but not least I would like to thank to my family and my friends for their love and support.

November 2019 **Anett GULYÁS**

CONTENTS

ACKNOWLEDGEMENT 3
ÖZET III
ABSTRACT V
SYMBOLS VII
ABBREVIATIONS IX
LIST OF FIGURES X
LIST OF TABLES XII
1. INTRODUCTION 1
1.1. PHOSPHORUS AND PHOSPHATE 1
1.1.1. IMPORTANCE OF PHOSPHORUS 1
1.1.2. Harms Related to Phosphate 2
1.1.3. Phosphorus Removal Technologies 2
1.1.3.1. Physical removal 2
1.1.3.2. Enhanced biological phosphorus removal (EBPR) 2
1.1.3.3. Chemical treatment 3
1.2. ADSORPTION 4
1.2.1. Adsorption process 4
1.2.2. P removal by adsorption 5
1.3. DESORPTION/ RECOVERY 6
1.4. ABOUT NANOTECHNOLOGY IN GENERAL 7
1.4.1. Nanomaterial 8
1.4.1.1. Classification of NM 9
1.4.1.2. Synthesis methods of NP 10
1.4.1.3. Characterization methods 11
1.4.2. Magnetic nanoparticles 11
2. MATERIALS AND METHODS 14
2.1. MATERIALS 14
2.1.1. Synthetic P solution 14
2.1.2. Dewatered Sludge Supernatant 14
2.2. METHODS 14
2.2.1. Synthesis of Magnetic Nanoparticles 14
2.2.2. Physicochemical characterization of Fe_3O_4 17
2.2.3. Adsorption experiments 19
2.2.4. Desorption experiments 22
2.2.5. Analytical methods 23
2.2.6. Validation of kinetic and isotherm models 24
3. RESULTS AND DISCUSSION 25

3.1. CHARACTERIZATION OF THE ADSORBENT 25
3.1.1. Point of zero charge 25
3.1.2. FT-IR results 26
3.1.3. XRD results 30
3.1.4. SEM results 31
3.1.5. EDX results 32
3.2. ADSORPTION PERFORMANCE 32
3.2.1. Effect of P concentration – equilibrium tests 32
3.2.2. Kinetic analysis 37
3.2.3. Effect of adsorbent dosage 40
3.2.4. Effect of pH 41
3.2.4.1. Adsorption of NH_4-N 42
3.3. DESORPTION EXPERIMENTS 43
3.3.1. Desorption of NH_4-N 48
4. CONCLUSIONS 49
REFERENCES 51
ÖZGEÇMİŞ 63

ÖZET

MANYETİK NANOPARTİKÜLLER KULLANILARAK KANALİZASYON ÇAMUR SÜZÜNTÜ SUYUNDAN FOSFOR GERİ KAZANIMI

Fosfor en temel besinlerden biridir, gübrelerin, deterjanların ve cilaların üretiminde kullanılır. Aşırı besin boşalmasından kaynaklanan çevre kirliliği, atık su arıtımında en önemli konudur. Besinler, yüzey suyu kaynakları, yeraltı suyu ve toprak üzerinde birçok olumsuz etki yaratır. Fosforun farklı sektörlerde yaygın olarak kullanılmasına rağmen, fosfor yenilenemez ve değiştirilemez sınırlı bir kaynaktır. Sonuç olarak, fosfatın geri kazanımı, uzaklaştırmanın yanı sıra dikkate alınmalıdır.

Bu çalışma, kanalizasyon çamuru süpernatanından fosfor gideriminde manyetik nanoparçacıkların (MNP'ler) kullanılmasının etkinliğini araştırmak için yapılmıştır. Çalışma kapsamında farklı parametrelerin demir oksit manyetik nanoparçacıkların kullanılmasıyla fosfat adsorpsiyonu üzerine etkilerini araştırmak için toplu deneyler yapıldı.

Demir oksit MNP birlikte çökeltme yöntemiyle hazırlanmıştır. MNP karakterizasyonu, X-ışını kırınımı, Taramalı Elektron Mikroskobu ve Fourier Transform İnfrared Spektroskopi ölçümleri ile yapıldı. Bu deneyler demir oksit MNP'nin etkili fosfat adsorpsiyonunu kanıtladı. Manyetik nanopartiküllerin yüzeyinde fosforun adsorbe olduğu varlığı, enerji dağıtıcı x-ışını spektroskopisi kullanılarak doğrulanmıştır. Partiküllerin yüzey yükünü farklı pH değerlerinde belirlemek için Zeta potansiyel ölçümleri yapılmıştır.

Denge çalışmaları, sentetik P çözeltisinin ve süpernatan çözeltisinin Redlich-Peterson izoterm modeliyle tutarlı olduğunu gösterdi. Sips modeli kullanılarak hesaplanan demir oksit MNP'nin teorik maksimum adsorpsiyon kapasitesi 20.8 mg / g'dir. Sentetik fosfat çözeltisinin ve süpernatan çözeltisinin kinetik çalışmaları, Elovich modeliyle tutarlıydı. En yüksek adsorpsiyon kapasitesi, 1000 mg/L P çözeltisi ve 0.3 g manyetik nanopartiküller ile ölçülmüştür. Fosforun demir oksit MNP yüzeyinden desorpsiyonu, MNP'lerin 1 saat boyunca 1 M NaOH çözeltisi ile işlenmesiyle etkili bir şekilde yapıldı.

Bu çalışmanın amacı, fosfatın adsorpsiyonu için MNP'yi değerlendirmektir. Fosfat geri kazanımı için daha ucuz ve daha uygun bir yöntemi incelemek için nanopartiküller için daha doğru bir kullanım bulmak istiyoruz.

Anahtar Kelimeler: Manyetik nanopartiküller, Fosfat giderimi, Fosfat geri kazanımı, Adsorpsiyon, Zeta potansiyeli

ABSTRACT

PHOSPHATE RECOVERY FROM SEWAGE SLUDGE SUPERNATANTUSING MAGNETIC NANOPARTICLES

Phosphorus is one of the most essential nutrients; it is used in the manufacture of fertilizers, detergents, and polishers. Environmental pollution due excessive nutrient discharges is the most important issue in wastewater treatment. Nutrients have many adverse effects on surface water resources, groundwater and soil. Despite the extensive uses of phosphorus in different sectors, phosphorus is a non-renewable and non-interchangeable limited resource. Consequently, the recovery of phosphate should be considered as well as the removal.

This study was carried out to investigate the efficiency of employing magnetic nanoparticles (MNPs) in phosphorus removal from sewage sludge supernatant. In the scope of the study, batch experiments were performed to investigate the effect of different parameters on phosphate adsorption using iron oxide magnetic nanoparticles.

The iron oxide MNP was prepared with co-precipitation method. MNP characterization was done with X-ray diffraction, Scanning Electron Microscopy and Fourier Transform Infrared Spectroscopy measurements. These experiments proved the effective phosphate adsorption by iron oxide MNP. The presence adsorbed of the phosphorus on the surface of magnetic nanoparticles was confirmed using energy-dispersive x-ray spectroscopy. Zeta potential measurements were conducted to determine the surface charge of the particles at different pH values.

Equilibrium studies showed that the synthetic P solution and supernatant solution was consistent with the Redlich-Peterson isotherm model. The theoretical maximum adsorption capacity of iron oxide MNP calculated using Sips model is 20.8 mg/g. The kinetics studies of the synthetic phosphate solution and supernatant solution was consistent with the Elovich model. The highest adsorption capacity was measured with 1000 mg/L P solution and 0.3 g magnetic nanoparticles. Desorption of phosphorus from the iron oxide MNP surface was effectively done by treating the MNPs with 1 M NaOH solution

for 1 hour.

The aim of this study to evaluate the MNP for the adsorption of phosphate. We would like to find a more accurate usage for nanoparticles, moreover to examine a cheaper, more available method for phosphate recovery.

Keywords: Magnetic nanoparticles, Phosphate removal, Phosphate recovery, Adsorption, Zeta potential

SYMBOLS

$\mathbf{C_e/C_0}$	: Equilibrium concentration (mg/L)
$\mathbf{C_i}$	: Initial concentration (mg/L)
$\mathbf{C_t}$	: Concentration at time, t (mg/L)
$\mathbf{D_{des}}$	: Desorption rates (%)
K	: Scherrer constant
$\mathbf{k_1}$	: Rate constant of pseudo-first order equation (1/min)
$\mathbf{k_2}$	: Rate constant of pseudo-second order equation (g/(mg·min))
$\mathbf{K_F}$	: Freundlich constant $((mg/g)/(mg/L)^{1/n})$
$\mathbf{K_L}$	: Langmuir constant (L/mg)
KR	: Redlich-Peterson constant
$\mathbf{K_R}$	: Redlich-Peterson constant
$\mathbf{K_S}$	: Sips constant $(mg/L)^{(-1/nS)}$
m	: Mass (g)
n	: Freundlich intensity parameter
NRMSE	: Normalizes root mean square error
$\mathbf{q_a}$	: Initially adsorbed PO_4^{3-} (mg/g)
$\mathbf{q_{calc}}$	: Calculated amount of adsorbate uptake (mg/g)
$\mathbf{q_d}$	: Amount of desorbed uptake (mg/g)
$\mathbf{q_e}$	: Amount of adsorbate uptake at equilibrium (mg/g)
$\mathbf{q_{exp}}$	: Amount of adsorbate uptake, experimental (mg/g)
$\mathbf{Q_{max}}$	: Maximum adsorption capacity calculated from Langmuir model (mg/g)
$\mathbf{q^S_m}$	: Maximum adsorption capacity calculated from Sips model (mg/g)
$\mathbf{q_t}$	: Amount of adsorbate uptake at time, t (mg/g)
R%	: Removal efficiency %
$\mathbf{R^2}$	: Correlation coefficient
T	**:** Temperature (°C)
t	**:** Time (min)
V	: Volume (L)
W	: Weight (g)

$\mathbf{X^2}$	: Chi square
$\boldsymbol{\alpha}$	: Initial sorption rate (mg/g·min)
$\boldsymbol{\beta}$	: Elovich constant (g/mg)
$\boldsymbol{\beta}$	: Line broadening at half maximum, FWHM (Radians)
$\boldsymbol{\theta}$	: Diffraction angle (°)
$\boldsymbol{\iota}$	: Size of the crystalline domains (nm),
$\boldsymbol{\lambda}$	: X-ray wavelength (Å)

ABBREVIATIONS

APR : average pore radius

ATP : Adenosine Triphosphate

BET : Brunauer-Emmett-Teller method

EBPR : Enhanceh biological phosphate removal

COD : Chemical Oxygen Demand

DI : Deionized water

EDS : energy dispersive spectroscopy

FTIR : Fourier Transform Infrared Spectroscopy

ICP-OES : Inductive Couples Plasma – optical emission spectroscopy

INTs : iron oxide nanotubes

JCPDS : Joint Committee on Powder Diffraction Standards

MIO : magnetic iron oxide

MIONs : magnetic iron oxide nanoparticles

MNPs : Magnetic Nanoparticles

MRI : Magnetic Resonance Imaging

NM : nanomaterial

NPs : Nanoparticles

nZVI **:** Nanoscalezerovalentiron

P : Phosphate

PAOs : Polyphosphate accumulating organisms

PFO : Pseudo-First Order

PSO : Pseudo-Second Order

RO : Reverse osmosis

SA : surface area

SEM : Scanning Electron Microscopy

SPIONs : super paramagnetic iron oxide nanoparticles

TEM : Transmission electron microscope

USPIOs : ultra-small super paramagnetic

XRD : X-ray Diffraction

LIST OF FIGURES

Figure 1.1. Adsorption……..…5
Figure 1.2. Figure Synthetic methods for NPs…...…….10
Figure 1.3. MNP Co-precipitation...……...10
Figure 1.4. Chemical structure of magnetite……...……...…….13
Figure 2.1. MNP synthesis……..15
Figure 2.2. Electric furnace…….16
Figure 2.3. Grinding machine…….16
Figure 2.4. Separation…….17
Figure 2.5. FT-IR and SEM machines...…….19
Figure 2.6. Batch…….20
Figure 2.7. Flow diagram of adsorption experiments……..…21
Figure 2.8. Magnetic separation…….22
Figure 2.9. Flow diagram of desorption experiments…….23
Figure 3.1. Zetapotential versus pH……...…….....25
Figure 3.2. FTIR spectra of raw MNP (a) and MNP after adsorption with synthetic P solution (b)…….……..27
Figure 3.3. FTIR spectra of raw MNP (a), after adsorption of NH_3-N (b) and after adsorption with supernatant (c)……29
Figure 3.4. X-ray diffraction pattern of MNP……...……..30
Figure 3.5. SEM image…...…….…….…..31
Figure 3.6. EDX results……...……...32
Figure 3.7. Effect of initial phosphate concentration…….33
Figure 3.8. Redlich-Peterson isotherm model for synthetic phosphate solution and supernatant……..36
Figure 3.9. Elovich kinetic model of phosphate solution adsorption……...……..39
Figure 3.10. Phosphate removal efficiency by MNP and adsorption capacity as a function of adsorbent dose …….....41
Figure 3.11. Removal efficiency with different initial pH…….42
Figure 3.12. Efficiency of PO_4-P adsorption/ desorption in each cycles (500 mg/L)….44
Figure 3.13. Efficiency of PO_4-P adsorption/ desorption in each cycles (1000 mg/L)..45

Figure 3.14. Efficiency of PO_4-P adsorption/ desorption in each cycles (10 g/L MNP)46
Figure 3.15. Efficiency of PO_4-P adsorption/ desorption in each cycles (15 g/L MNP)46
Figure 3.16. Efficiency of PO_4-P adsorption/ desorption in each cycles (20 g/L MNP)47
Figure 3.17. Efficiency of PO_4-P adsorption/ desorption in each cycles (25 g/L MNP)47

LIST OF TABLES

Table 1.1. Iron oxides……..……..11

Table 2.1. Parameters of the supernatant……14

Table 2.2. Validation parameters used for model evaluation……..24

Table 3.1. Equilibrium adsorption isotherms' parameters……..35

Table 3.2. Comparison of phosphate adsorption capacity of MNP……36

Table 3.3. Evaluation of kinetic models for P adsorption by MNP……...38

Table 3.4. NH_4-N concentrations of supernatant after adsorption……..43

Table 3.5. Adsorption results of NH_4 solution……43

Table 3.6. NH_4-N concentrations in NaOH solution after 5 adsorption-desorption cycles…….....48

1. Introduction

1.1. Phosphorus and Phosphate

Phosphorus is the 17th most abundant element in the universe and the 11th most abundant element in the earth crust; moreover there are about 200 phosphorus minerals that are known. Phosphorus is mostly appearing as white or red. The first one is more reactive. Phosphates are the fully oxidized form (oxidation number +5) of phosphorus. In water it occurs as PO_4^{3-}, $H_2PO_4^-$ and HPO_4^{2-}. Plants are able to assimilate the last two forms. In wastewater the following phosphates forms can be found organic phosphate, inorganic phosphate and polyphosphate (Toy, 1973). The concentration of phosphorus changes with the nature of the wastewater, such as municipal wastewater can contain 4-15 mg/L PO_4^{3-}, domestic wastewater has about 10-30 mg/L PO_4^{3-} and treated sewage has 1-5 mg/L of PO_4^{3-} (Markeb et al., 2016).

1.1.1. Importance of Phosphorus

Phosphorus is one of the most essential nutrients, essential for the transformation of Adenosine Triphosphate (ATP-energy transfer) and the creation of nucleotides. It has important role in reproduction and it is an advanced glue in molecules (Köbel, 2017; Farber, 1966). Additionally, it has importance in part of skeleton structures and of teeth (Juhászné and Dojcsákné, 2012; Sarıbuğa, 2014). It has industrial usage as fertilizers, water treatment, water softening, detergents, flame retardants, corrosion inhibitors paints, food and beverage, polishers and pharmaceuticals (Westheimer, 1987).

Environmental pollution due to excessive nutrient discharges is the most important issue in wastewater treatment. Nutrients have many adverse effects on surface water resources, groundwater and soil. In contrast, even though the extended uses of phosphorus in different sectors, phosphorus is a nonrenewable and non-interchangeable finite resource. According to studies we have reserve for 50-100 years (Cordell et al., 2019; Mandel et al., 2013). Consequently, the recovery of phosphate should be considered as well as the removal.

1.1.2. Harms Related to Phosphate

Discharged nutrients as nitrogen and phosphorus into surface waters cause eutrophication, which is harmful. Eutrophication is a cause of environmental and economic problems and it is dangerous for public health (Sawyer et al., 1994). Eutrophication is derived from the Greek ‘eu’ – well and ‘trephein’ – nourish words. When nutrients are oversupplied it causes excessive algae growth and toxic algae blossom. Therefore, oxygen depleted or hypoxic zones are developed (Carpenter et al., 1998). It will damage the aquatic life, causes fish kills, there can be changes in plant and animal species composition, the biodiversity can decrease, and the food webs can be disturbed (Franco et al., 2017). The reduction of the eutrophication is possible just under 10 mg/L phosphate concentration (Dryden and Stern, 1968).

1.1.3. Phosphorus Removal Technologies

The adsorbents which are used for phosphorus removal have to have high adsorption rate, high potential of practical application and should be easily recyclable (Onyango et al., 2007; Urano and Tachikawa, 1991).There are many studies about finding an effective method for phosphorus removal, such as chemical precipitation, biological treatment and physical removal.

1.1.3.1. Physical removal

For physical treatment the important factor is the size of the pollutant, this treatment has two types; sedimentation and filtration. In the case of sedimentation, they are using the gravity and based on the precipitation of hardly dissoluble phosphorus. For filtration we can use a membrane or sand filtration on which the solids cannot pass through. Reverse osmosis (RO) is a type of filtration which uses the force of the pressure that is higher than osmotic pressure through a semi-permeable membrane or filter (Choi, 2016).

1.1.3.2. Enhanced biological phosphorus removal (EBPR)

During biological treatment polyphosphate accumulating organisms (PAOs) are used to turn nutrients into a simple end product (Welles, 2016). In this process the biological system stimulates the growth of bacteria and in this way the bacteria will hold a huge amount of inorganic phosphate, and its name is biomass. The biomass can be easily removed by sedimentation. EBPR is achieved by submitting activated sludge to alternat-

ing anaerobic and aerobic/anoxic conditions. In anaerobic environment PAOs release orthophosphate and in aerobic environment they pick up orthophosphate (Choi, 2016). Phosphorus removal is achieved by wasting the excess sludge with phosphate accumulating organisms having high level of poly-P (4-12%). Effluent P levels in the range 0.5-2 mg/L could be achieved with EBPR process.

1.1.3.3. Chemical treatment

This operation includes chemical coagulation, adsorption and chemical precipitation. These are unit processes and built up from different level as; preliminary, primary, secondary, advanced and disinfection (Bowker and Stensel, 1990). On these different levels different matters are removed; in preliminary rags and floatables; primary suspended solids and organic matters; secondary biodegradable organic matter, suspended solids and P and on tertiary level residual suspended solids are removed. During precipitation different metal salts are added such as; $FeCL_3 \cdot 6H_2O$ (ferric-chloride) and $NaAlO_2$ (sodium-aluminate). After adsorption these materials become $FePO_4$ (iron (III)-phosphate) and $AlPO_4$ (aluminum-phosphate). After the procedure they are easily removable with sedimentation or filtration. The optional pH for precipitation for Fe^{3+} salts is 4.5-5, nevertheless this cannot be reached, but they are quite effective on pH 7-8 too. To precipitate 1 g of PO_4^{3-} and reach 90 % of efficiency, 6-8 g of Fe^{3+} is needed.

$$Me^{3+} + PO_4^{3-} \rightarrow MePO_4 \quad (1.1)$$

Each of these methods has their own advantages and disadvantages in practice (Jeongyun et al., 2016). Although chemical precipitation is resulted with highest removal efficiency and lowest effluent P, high sludge production and cost of chemical addition make the process unfeasible for many cases. Biological treatment is not the best option because of the fluctuating characteristics of water. The EBPR method's disadvantage is that if the air circulation is not adequate the phosphate can get back to the water treatment system (Markeb et al., 2016).

In the last years, environmental researches have started to pay more attention about the use of functionalized magnetic nanoparticles. These nanoparticles can be magnetic nanoparticles, mainly nano zero-valent iron, magnetite (Fe_3O_4) and maghemite (γ-Fe_2O_3) nanoparticles (Giang et al., 2015). In the study of Jeongyun et al. (2016), they examined

the recovery of phosphate with the use of magnetic iron oxide (MIO) and iron oxide nanotubes (INTs) with artificial wastewater (Jeongyun et al., 2016). Magnetic iron oxide and iron oxide nanotubes are chosen as potent substitute, due to the iron oxide particles can simply be isolated from the solution using magnets and an INT fixed on the surface of the iron foil is not inevitable for IO recovery. Furthermore, the adsorbed phosphate can be successfully desorbed with solutions pH above 7. Onto P recovery, iron oxide particles need magnetic recovery equipment, though, when INT was used for phosphate restoration, additional recovery step is not needful. The two strategies demonstrated powerful adsorption performance for phosphate recovery in wastewater (Jeongyun et al., 2016). A magnetic adsorbent includes two advantages, magnetic and adsorption can be applied to adsorb pollutants and subsequently remove the pollutants from the solution by a magnetic separation technology without using centrifugation or filtration (Jiang et al., 2017).

1.2. Adsorption

German physicist Heinrich Kayser coined the term "adsorption" in 1881. Adsorption is defined as the adhesion of a chemical species onto the surface of particles. The material that gets adsorbed on the surface is known as adsorbate and the surface on which adsorption happens is known as adsorbent. Adsorption has two types; chemical adsorption (chemisorption) and physical adsorption (physisorption). Physisorption is caused mostly by van der Waals forces and electrostatic forces, low heat adsorption, non specific, molecular structure is not changing so it is reversible and takes places as multilayer. In contrast, chemisorption is caused by ion change, electrostatic attraction; chelating formation it means strong attraction cause of this it’s hardly reversible. It is a high heat adsorption, take places as monolayer; molecular structure is changing and mostly specific (Hacıosmanoğlu, 2019; Sawyer et al., 1994).

1.2.1. Adsorption process

The steps of adsorption are: bulk, film and intraparticle transport and the adsorption of the solutes on the active sites (Figure 1.1). The physical and chemical properties of the adsorbent and the environmental circumstances play important rule in the type of adsorption mechanism. There a lot of parameters which affects the adsorption process, these are the characteristics of the sorbent (surface charge, area, etc.), the adsorbate

(molecular weight, size, solubility, etc.) and the solution (pH, ionic strength, temperature, etc.) moreover the duration of the adsorption (Loganathan et al., 2014).

The highest quantity of adsorption is significantly dependent on the surface area and the pore size (Markeb, 2017).

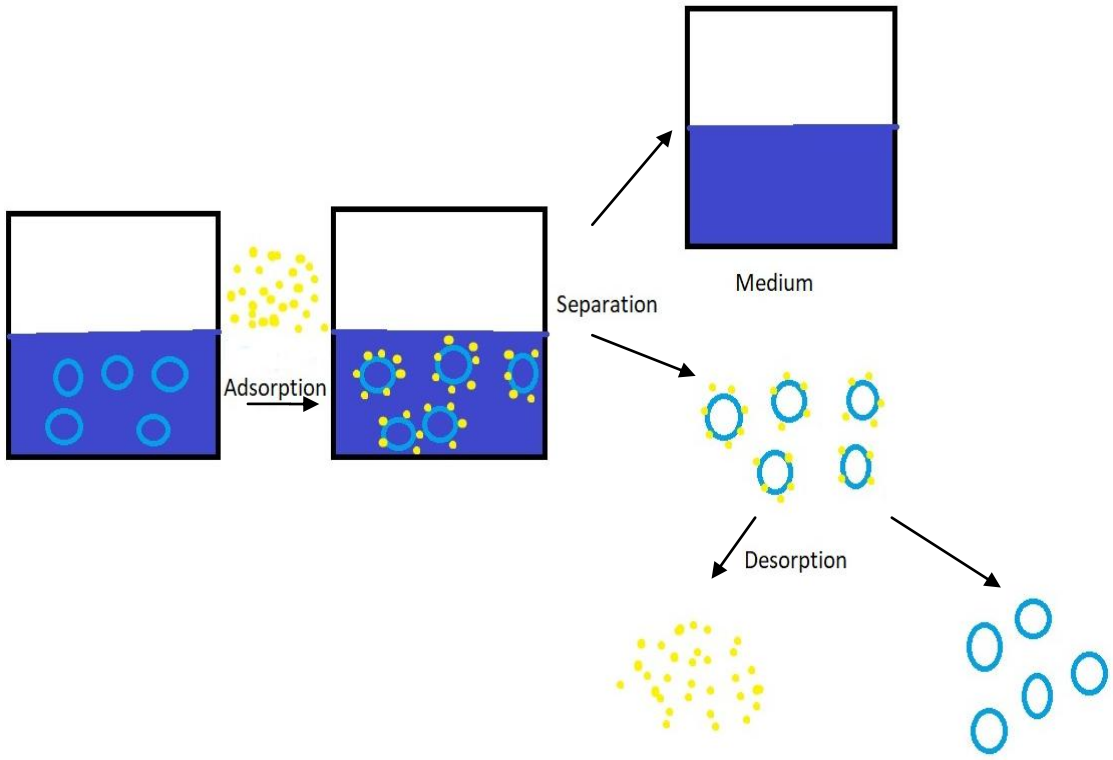

Figure 1.1. Adsorption

1.2.2. P removal by adsorption

For phosphate removal by adsorption several studies were carried out (Chitrakar et al., 2006; Genzet al., 2004; Lueng et al., 2006; Zach-Maor et al. 2011a; Zeng et al., 2004) and all of them proved that P removal by adsorption is quite an effective way. Furthermore, adsorption is a well established technology for water and wastewater treatment. The previous studies showed that there are more and more selective and cost effective sorbents that can be developed. In contrast with the chemical precipitation this technique does not produce large volumes of chemical sludge. Various types of phosphorus adsorbents made from zeolites (Geelhoed et al., 1997), lanthanum and yttrium compounds (Wasay et al., 1996; Zhang et al., 2015), aluminum compounds (Gao et al.,

2013; Guaya et al., 2015; Kabayama et al., 2003; Kabayama et al.,2005; Oliveira et al., 2011), zero-valent iron (Wu et al., 2013), amine-functionalize, $Pr(OH)_3$ (Tang et al., 2014), magnesium amorphous calcium carbonate (Xu et al., 2014), zirconium compounds (Su et al., 2015; Zong et al., 2013) and iron (III) oxide compounds (Bastin et al., 1999; Lakshmanan et al., 2014; Lin et al., 2013; Lueng et al., 2006; Markeb at al., 2016; Zach-Maor et al., 2011a; Zeng et al., 2004; Zhu et al., 2013) were studied.

1.2.2.1. Sorption mechanism

The sorption mechanism regulates the capacity, energy and kinetics of adsorption of phosphate. There are five mechanisms which are: ion exchange, hydrogen bonding, surface precipitation, diffusion and ligand exchange. Ligand exchange is a type of chemisorptions, it is strong and fast, and not always reversible and zeta-potential is reduced with increasing pH. During ligand exchange the sorbing anion bonds with the metallic anions by covalent bond, in this way the already bonded OH ions are released. The advantage for ligand exchangers is that they can extract high percentage of anions having higher selectivity for adsorption from very dilute solutions of the anions even in the presence of competing anions of lower selectivity. In this way P is able to form inner sphere complexes at the surface of iron oxide, which can be monodentate, bidentate, mononuclear or binuclear (Loganathan et al., 2014).

1.3. Desorption/ Recovery

According to Cordell et al. (2011) 30 types of methods of phosphorus recovery from sewage sludge exist, the most uncomplicated one is the immediate use of activated sludge as manure (Cordell at al., 2011; Li et al., 2014; Xie et al., 2010).

As well sewage sludge can include important quantity of possibly dangerous organic pollutants (Suciu et al., 2015; Tarayre et al., 2016; Zhou et al., 2016). The laws about the heavy metal in the sludge are very strict because of this the techniques for sludge treatment and indirect recovery of phosphorus are turning into more and more popular.

Many parameter like pH, COD (chemical oxygen demand), P, Mg and K amount, temperature, time and intensity of oxygenation have an important influence on the efficiency of the progress of desorption (de-Bashan and Bashan, 2004; Havukainen et al., 2016).

Sewage sludge treatment and recycling was described in some studies before. In the work of Johansson et al. (Johansson et al., 2008) the method was applied in restoration, composing, hygienisation and agricultural use.

1.4. About Nanotechnology in General

The XXI. Century's technical novelty is the 'nano'. This technology has been developed and appeared in most of economic sectors. The nanotechnology is used in a wide scope of activities, for example in analytics, electronics, biomedical applications, environmental industry and in power generation (Köbel, 2007). A material science-based part of nanotechnology is nanomaterials, its analyzing materials on nanoscale. Types of nanomaterials are nanoparticles, which has different, highly increased surface area ratio (Sarıbuğa, 2014). These nano-scale particles have significance in medical biology and chemical industry too. Nano-sized iron oxide particles are nontoxic supermagnetic materials, furthermore because of their small size they have untapped great potentials (Juhászné and Dojcsákné, 2012). Likewise, their efficient use in membrane separation, water treatment and purification processes have been presented.

Firstly, in the history William Fullarton used a magnet to detach iron minerals, he defined the magnetic separation in 1792 (Yavuz et al., 2009)**.** Magnetic separation techniques are widely used in diverse areas from steel production to biotechnology. These methods are commonly used because they are fast, cost effective and highly productive (Cao et al., 2006). They have advantages during centrifugation, filtration and solid-phase extraction.

Towler et al. (1996) reported heavy metal recovery from seawater samples by magnetic sorbent (Towler et al., 1996). Magnetic nanoparticles can effectively remove heavy metal ions because they can capture and transport them. According to this in the last years scientists released more and more studies about the usage of MNPs. In a while they started to examine these particles for biomedical applications too. For instance, nanoparticles have shown well-seeming performance in contaminant takeout or toxicity reducing. Furthermore, their impressive usage in membrane separation water treatment and cleaning courses have been demonstrated.

The application of nanotechnology in the medical fields has been spreading in the last years. Especially in sectors as drug delivery where the target is to lead the drug to the

disease site with slightest unwanted secondary effect and to decrease the dosage by more localised and efficient targeting. This involves magnetic drug targeting, whereby an external magnetic field gradient is applied at the target tissue to deliver the drug through active targeting using high-affinity ligand attachment, as well as therapeutic strategies (Fatima and Kyo-Seon, 2018).

In the result of phosphorus removal and recovery from wastewater, magnets can be made of iron, cobalt and nickel. Iron is the most used one, it has a lots of natural phases and the most suitable magnetic nanoparticles are Fe_3O_4 and γ-Fe_2O_3 and nanoscale zerovalent iron (nZVI).

In the United States, many practical experiences of site remediation using nZVI has been reported (Comba et al., 2011; Su et al., 2012). In Europe, although only three full scale applications were reported, there were many pilot-test projects with the application of nZVI for various contaminants (Mueller et al., 2012).

Magnetic nanoparticles have different physicochemical characteristic, these are caused by the difference in their iron oxidation states and their ability for pollutant removal. Out of nZVIs, magnetite (Fe_3O_4) with both Fe(II) and Fe(III), has been examine the most, it is the favored type because of the presence of the Fe^{2+} statewith the potential of acting as an electron donor.

1.4.1. Nanomaterial

Nanomaterials have requirements: greatly small size, wished shape, high specific surface area, high surface area to volume ratio, high catalytic capability, charge opposite to targeted contaminants, large number of active sites for pollutants adsorption, strong mechanical feature, nanotoxicity, magnetic in nature for easily separating from final effluent, supermagnetic in nature and can be produced in bulk amount (Srivastava et al., 2015).

Nanomaterials are generally considered to have a particle size of between 1 and 1000 nm. Nanostructures can be called a material if it contains independent structural units which size is in the nanometer size range.

They have three layers, according to Shin et al., (Shin et al., 2016) the surface layer, which may be functionalized with a variety of small molecules, metal ions, surfactants and polymers. The shell layer is chemically dissimilar material from the core, which is

basically the central part of the NP and usually attributes the NP itself.

The application of magnetic nanoparticles is very wide, they can be successfully used to produce magnetic fluids, to develop magnetic storage media, to catalyze reactions and to treat wastewater. Another very important field of usage is medicine. In medication MNPs firstly have been used in MRI as contrast material. Furthermore they can be used for hyper-terminal treatment of tumors, as biosensors and as drug and gene delivery systems. These materials are successfully applied in cosmetology, dermatology, dental implantology, and orthopedics and in surgery. The essential part of the drug delivery is to direct the MNPs together with the drug substance to the desired location by magnetic field and hold it there until the end of the treatment (Ramsden, 2009).

Moreover water treatment technologies apply MNPs. Due to their high specific surface area, the particles are capable of adsorbing organic matter and heavy metal ions in water. As a result of their magnetic properties, their removal is relatively simple, with a permanent magnet, The material has been bound on the surface of the removed particles has several methods, for example, can be easily removed by chemical removal or by mild heat treatment (Ábraham, 2016).

1.4.1.1. Classification of NM

Nanomaterials have been classified and grouped in a number of ways (they can be natural/synthetic; or according to their dimensionality, morphology, composition, uniformity and agglomeration). Synthetic nanomaterials have four groups; such as carbonaceous, metal based, dendrimers, composites (Markeb, 2017).

1.4.1.2.Synthesis methods of NP

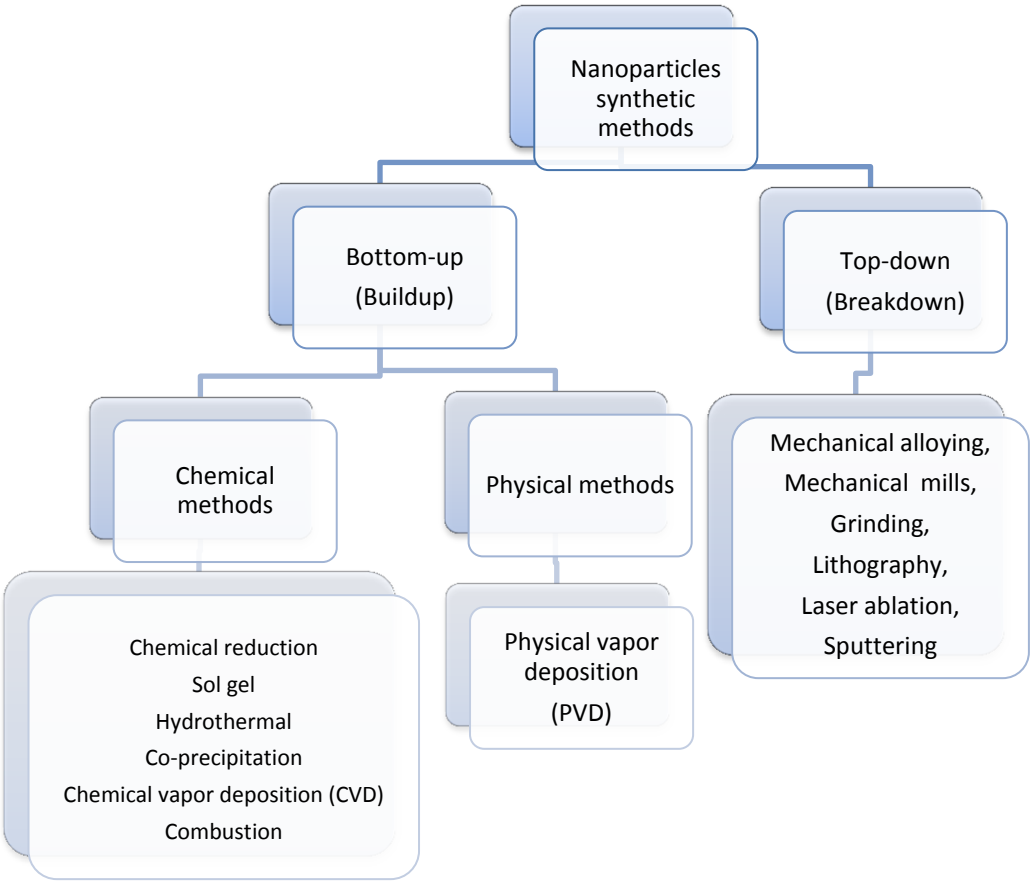

Figure 1.2. Synthesis methods for NPs, (adapted from: Horikoshi and Serpone, 2013)

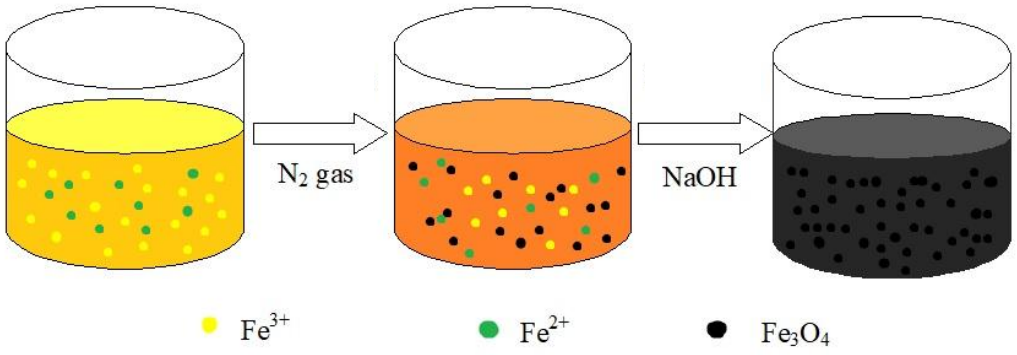

Figure 1.3. MNP Co-precipitation

1.4.1.3. Characterization methods

Scanning electron microscopy (SEM) is used for the characterization of the surface morphology of the adsorbents (Lalley et al., 2016). Fourier transform infrared (FTIR) spectroscopy can access to the functional groups of the P.

With X-ray diffraction (XRD) the crystal structure of the MNP can be characterized (Jeongyun et al., 2016).

Trasmission elentron microscope (TEM) and energy dispersive spectroscopy (EDS) can be used together to identify the size of the NM.

Zeta potential determines the surface charge of each the sorbent.

The morphology and physical properties of the sorbents can be studied using a transmission electron microscopy (TEM) (Wu et al., 2017).

Inductive Couples Plasma – optical emission spectroscopy (ICP-OES) is a technique in which the composition of elements in (mostly water-dissolved) samples can be determined using plasma and spectrometer (Markeb, 2017).

Elemental (C, H, N) analyses can be conducted using an EA112 CHN elemental analyzer (Chen et al., 2011).

Physical adsorption: Pore and surface characteristics were measured by N_2 adsorption. The surface area (SA) and average pore radius (APR) can be determined by multipoint.

1.4.2. Magnetic nanoparticles

Iron is one of the most common elements on Earth. It can be found in nature in many rocks in the form of different silicates and oxides. Iron can form multiple compounds with oxygen that have different properties.

Table 1.1. Iron oxides (Adapted from Cornell and Schwertmann, 2000)

Name	Magnetite	Maghemite	Hematite	Wüstite	Goethite
Magnetic property	ferro-magnetic	ferro-magnetic	antiferro-magnetic	antiferro-magnetic	antiferro-magnetic
Formula	Fe_3O_4	γ-Fe_2O_3	α-Fe_2O_3	FeO	α-FeOOH
Color	black	brown	red	grey	yellow

These iron-oxides can turn to each other under appropriate circumstances; these transformations can be for example realignment, oxidation, and dehydration. Among the nanoscale supermagnetic iron oxide compounds, magnetite (Fe_3O_4) and maghemite (γ Fe_2O_3) are at the center of biological research, they used to form a core of magnetic iron oxide nanoparticles (MIONs). Magnetite is a mixed oxide, which means that it also contains iron atoms with oxidation state II and III in a ratio of 1: 2. Accordingly, the formula is $FeO \cdot Fe_2O_3$. It is a material with ferromagnetic properties; therefore it can be magnetized and then becomes a permanent magnet itself. Maghemite (γ-Fe_2O_3) contains brown ferromagnetic iron oxide, contains only iron ions with oxidation state III (Ábraham, 2016).

In addition to minerals, magnetite is found in various biological systems, such as magnetotactic bacteria. These bacteria have a cell organ called a magnetosome, which is responsible for the synthesis of crystals. These crystals have narrow size distribution and definite morphology. This morphology is different from the magnetite particles obtained by laboratory synthesis, so that the particles can serve as a kind of biomarker (Kósa and Pósfai, 2007).

It is important to note that the magnetic behavior of various iron oxide particles is highly dependent on the particle size. Magnetite nanoparticles exhibit ferromagnetic over about 20 nm, while they exhibit super paramagnetic behavior. Maghemitic particles are characterized by super paramagnetic behavior. An interesting aspect is the question of surface properties and the properties of molecules that can be attached to the surface. Studies have shown that carboxylic or amino group molecules are best bound to iron oxide particles (Cushing et al., 2004).

The magnetic property of a material is determined by the spin of its unmatched electrons. Magnetic materials are unique units of magnetic wear consist of domains (Szittya, 1999). The magnetic properties of the material are influenced by the amount of magnetic domains, and how the domains of the material react in the presence or absence of an external magnetic field. When a material consists of only one magnetic domain, it exhibits superparamagnetic characteristics.
Due to their dipole character, the domains are aligned in the same direction as the magnetic field - while in the absence of magnetic field they will have diffuse distribution as a

result of Brown Movement (Thorek et al., 2006).

This behavior can be observed in iron oxide particles also in a certain size range. The particles between 50 and 100 nm are classified into a group of super paramagnetic iron oxide nanoparticles (SPIONs), while sizes below 50 nm are called ultra-small super paramagnetic (USPIO) iron oxides (Boyer et al., 2010). Generally, nanoscale iron oxide particles have different coatings that help stability and improve application in, for example, biological systems.

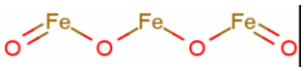

Figure 1.4. Chemical structure of magnetite

2. Materials and Methods

2.1. Materials

2.1.1. Synthetic P solution

Synthetic phosphate stock solution (1000 mg/L) was prepared by dissolving 2.177 g KH_2PO_4 and 0.028 g K_2HPO_4 in 1 L deionized water.

2.1.2. Dewatered Sludge Supernatant

Sludge supernatant was taken from Ataköy WWTP plant, Istanbul. The following tests were carried out to examine the important parameters of the supernatant (Table 2.1).

Table 2.1. Characterization of the supernatant

Parameter	Value (mg/L)
pH	~ 8.1
Mg^{2+}	3.74 (mg/L)
Ca^{2+}	3.50 (mg/L)
Chemical oxygen demand	381 (mg/L)
NH_3-N	590 (mg/L)
PO_4-P	166 (mg/L)

2.2. Methods

2.2.1. Synthesis of Magnetic Nanoparticles

The co-precipitation process was used in the synthesis of magnetite (Fe_3O_4) nanoparticles (MNP). Iron (III) (0.08 mol) and Iron (II) (0.04 mol) salts were dissolved in 700 mL deionized water, in a molar ratio of 2:1. This solution was mixed at 500 rpm and heated up to 60 °C under N_2 atmosphere. After the salt solution was reached to the desired temperature, NaOH (5 M) was added rapidly until the pH was 11. Formation of black precipitates was observed immediately after the addition of the base (Figure 2.1). The solution was allowed to stir at 500 rpm and at 60 ^{0}C for 30 min. Then, the solution

was left to cool down and washed with deionized water and ethanol several times till the pH decreased to 7.

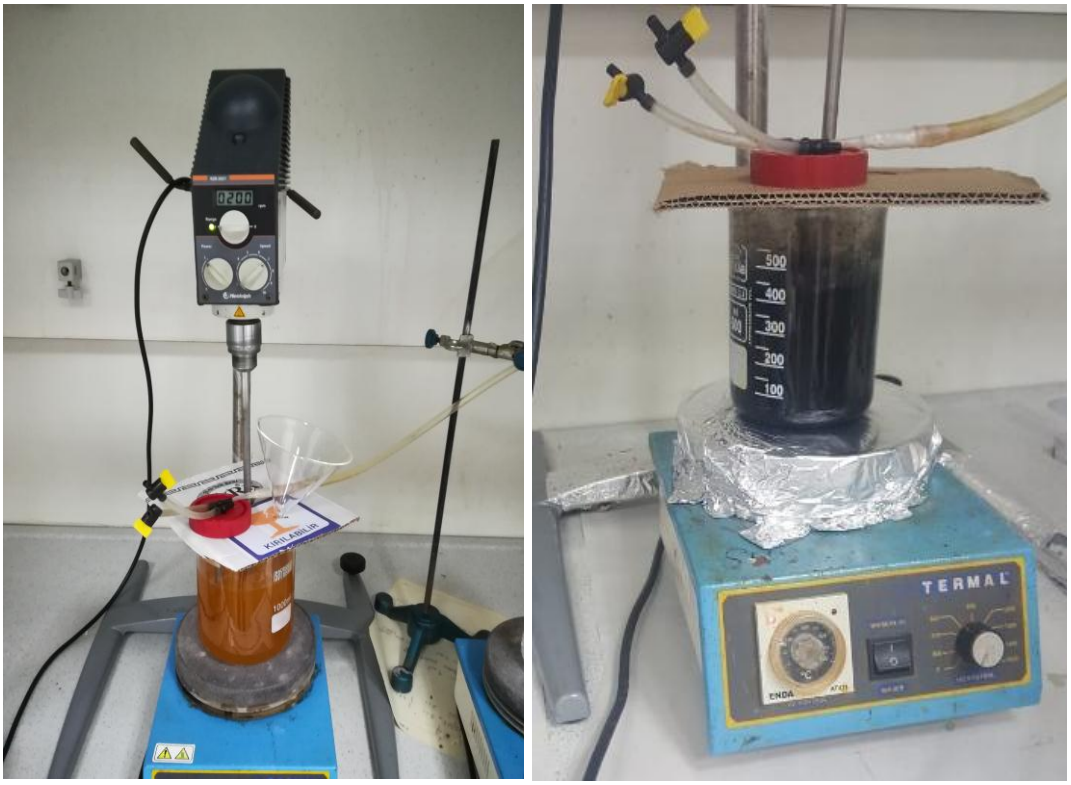

Figure 2.1. MNP synthesis

The black precipitates were dried in the electric furnace (Figure 2.2) under vacuum at 60 ^{0}C for 24 hours.

Figure 2.2. Electric furnace

After the drying step, the surface of the nanoparticles increased by using pestle and mortar as a first step. In order to break down the agglomerates formed during drying, powder was ground by beat beater with 0.5 mm grinding media (Figure 2.3).

Figure 2.3. Grinding machine

After the grinding process the separation of the beats and the grinded material was necessary (Figure 2.4). After this process the material was ready for usage.

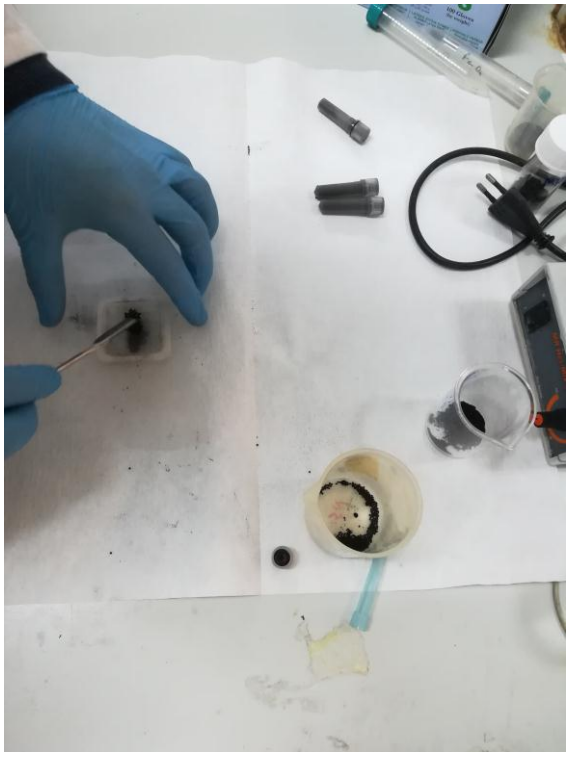

Figure 2.4. Separation

2.2.2. Physicochemical characterization of Fe_3O_4

To characterize the MNP, we used zeta potential measurements, FTIR, XRD, SEM and EDX, all have advantage to give different evidences for interpreting the adsorption mechanism of phosphate.

The pH_{zpc} is very useful parameter to understand the interaction between MNP and anionic phosphate ion, the adsorption mechanism of phosphate. Zeta potential parameter is a measure of surface charge and governs interactions with environmental media and biota. pH, ionic strength and dissolved organic matter has influence on the pH_{zpc}. This value indicates the degree of repulsion between adjacent, similarly charged particles, i.e., low values indicate poor stability and potential aggregation of particles. It is also used to determine the pH of the phosphorus solution in adsorption experiments, for this reason zeta potential analyzer (Malvern Instruments Zetasizer 2000) was used, with 1

mM KCl as background electrolyte.

Fourier transform infrared spectroscopy (FT-IR; Jasco FT/IR-4700) was used to investigate the phosphate interaction with MNP. It was performed with area of 4 cm^{-1}, using KBr method, by, under atmospheric air and vacuum conditions (Figure 2.5). All samples were recorded into the range of 4000-400 cm^{-1}. FTIR analysis shows the functional groups involved in the o-P binding to iron oxides and to find the type of inner sphere complex formed by o-P with the iron oxide surface (Arai and Sparks, 2001; Elzinga and Sparks, 2007; Parfitt and Atkinson, 1976; Persson et al., 1996; Russel et al., 1974) .

XRD (x-ray diffractometry) is one of the most important characterization methods to find the structural properties of nanoparticles. It gives enough information about the crystallinity and phase of NPs (Chitrakar et al., 2006). The XRD analysis was employed to determine the average particles size (by Scherer formula) of Fe_3O_4 MNPs after excitement with Cu-Kα radiation at and, wavelength 0.154 nm and 2θ range at (5° - 105°). In this study x-ray diffraction was performed for raw magnetic iron oxide by Rigaku XRD apparatus.

SEM (scanning electron microscope) was used for the characterization of the surface morphology and to define particles size of the MNP (Lalley et al., 2016). Energy dispersive X-ray spectrometry (EDX) was used to determine Fe:P molar rations in vivianite (Miot et al., 2009). For SEM and EDX we used Zeiss EVO MA10 (Figure 2.5).

As an additional experiment, Mg^{2+} and Ca^{2+} were measured with photoelectric flame photometer, Perkin Elmer AAS 400.

Figure 2.5. FT-IR (left) and SEM (right)

2.2.3. Adsorption experiments

Adsorption of phosphate ion onto magnetite was examined under batch conditions (figure 2.6). For pH adjustment 2M HCl solution was used. MNP was added to phosphate samples 20 mL of aqueous phosphate samples and treated in ultrasonic bath (Bandelin SONOREX digital 10p) for 10 minutes to evenly distribute magnetite nanoparticles. The samples were placed into a temperature-controlled shaking incubator (IKA, Germany) at fixed speed of 250 rpm and room temperature (25 °C), in 25 mL glass flaks. Before chemical analyses, magnetite particles were attracted using a magnet and the solution phase filtered through 0.45 μm membrane filters (Figure 2.6; 2.7).

The first tests were conducted as a function of the initial P concentration in synthetic P solution. The initial concentrations of the samples were adjusted between from 25-1000 mg/L. In this experiment, pH was initially set to ~3. For equilibrium studies, 0.3 g magnetic nanoparticles were added to P solution, the other conditions were the same as it is described at the previous part.

The second set of experiments was performed to examine the adsorption kinetic by different contact times (1, 15, 30, 45, 60, 90, 120, 180, 240, 300, 1260 and 1440 minutes), with both synthetic P solution (~500 mg/L of initial P; pH ~3) and supernatant (~136 mg/L of initial P; pH ~5). Adsorption kinetic experiments conducted with, 0.3 g magnetic nanoparticles, other conditions were the same as it is described at the first part.

Third set of tests were carried out to examine the connection between the adsorbent dosage and P adsorption with supernatant batch test at various initial concentrations of MNP (0.1, 0.2, 0.3, 0.4 and 0.5 g). At this test initial P concentration was ~136 mg/L and pH adjustment was done until pH reached ~5, other conditions were the same as it is described at the first part.

The fourth set of experiments was conducted to see the effect of pH on P adsorption capacity, with supernatant at initial P concentration ~166 mg/L and 0.3 g MNP. The initial pH of the supernatant was 8.1, and after adding 3.7 mL of 2M HCl solution to the solution, initial pH decreased to ~5. The other experimental conditions were the same as previously described

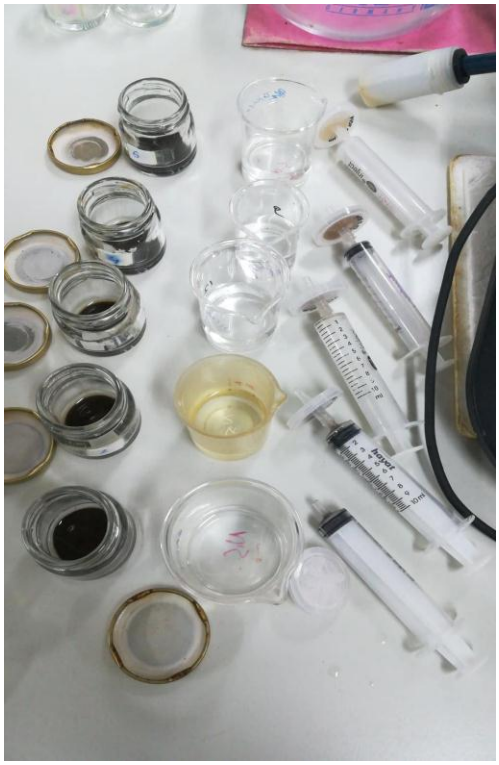

Figure 2.6. Batch

Figure 2.7. Flow diagram of adsorption experiments

The amount of phosphate adsorbed (mg/g or mg P/g) were calculated based on the mass balance equation given below:

$$q = \frac{(C_0 - Ceq) \times V}{W} \quad (2.1)$$

where q is the adsorbent capacity (mg/g); C_0 is the initial concentration of anions in solution (mg/L); C_{eq} is the final or equilibrium concentration of anions in solution (mg/L); V is the volume of experimental solution (L); and W is the weight of adsorbent (g) (Jiang et. al., 2013).

Removal efficiency was calculated as:

$$R\% = \frac{(C_o - C_e)}{C_o} * 100 \quad (2.2)$$

where, C_o is the initial P concentration and C_e is the final P concentration (mg/L)

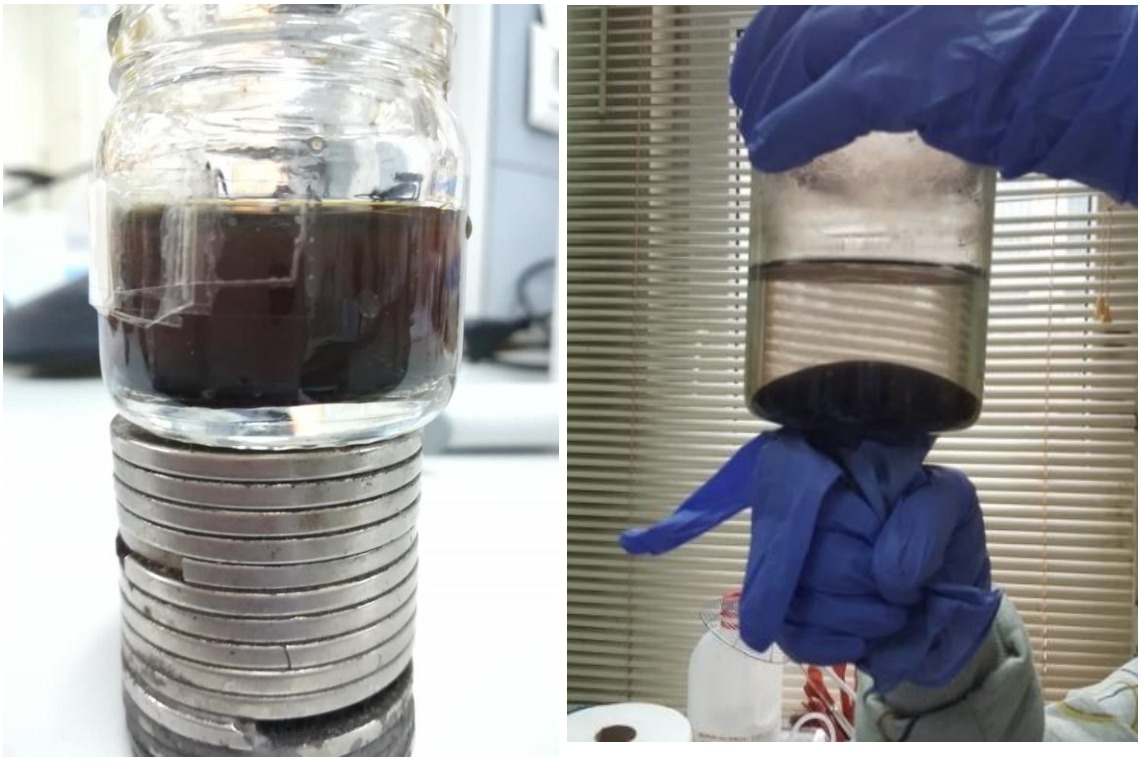

Figure 2.8. Magnetic separation

2.2.4. Desorption experiments

Desorption experiments carried out to evaluate phosphorus recovery potential and reusability of MNPs. Preliminary experiments conducted to find the necessary contact time in desorption experiments. In some desorption experiments, same NaOH solution was used repeatedly to obtain concentrated phosphorus solution. In each cycle, after adsorption 20 mL of NaOH was added during desorption tests and shaked (250 rpm) for 1 hour at room temperature. Flow diagram of the desorption experiments is given in Figure 2.9. Desorption of phosphorus from MNP carried out at room temperature with 1h contact time and 1 N NaOH solution. Different amounts of MNP was used in the experiments with supernatant (0.2, 0.3, 0.4, 0.5 g) and synthetic P solution (0.3 g). We repeated the adsorption-desorption process 9 times for evaluating the reusability of the magnetic nanoparticles. Adsorption performance was tested after each desorption experiment.
Desorption rates (%) were calculated according to the following expression,

$$D_{des} = \left(\frac{q_d}{q_a}\right) * 100 \qquad (2.3)$$

where, q_d is the desorbed PO_4^{3-} (mg/g) and q_a is initially adsorbed PO_4^{3-} (mg/g).

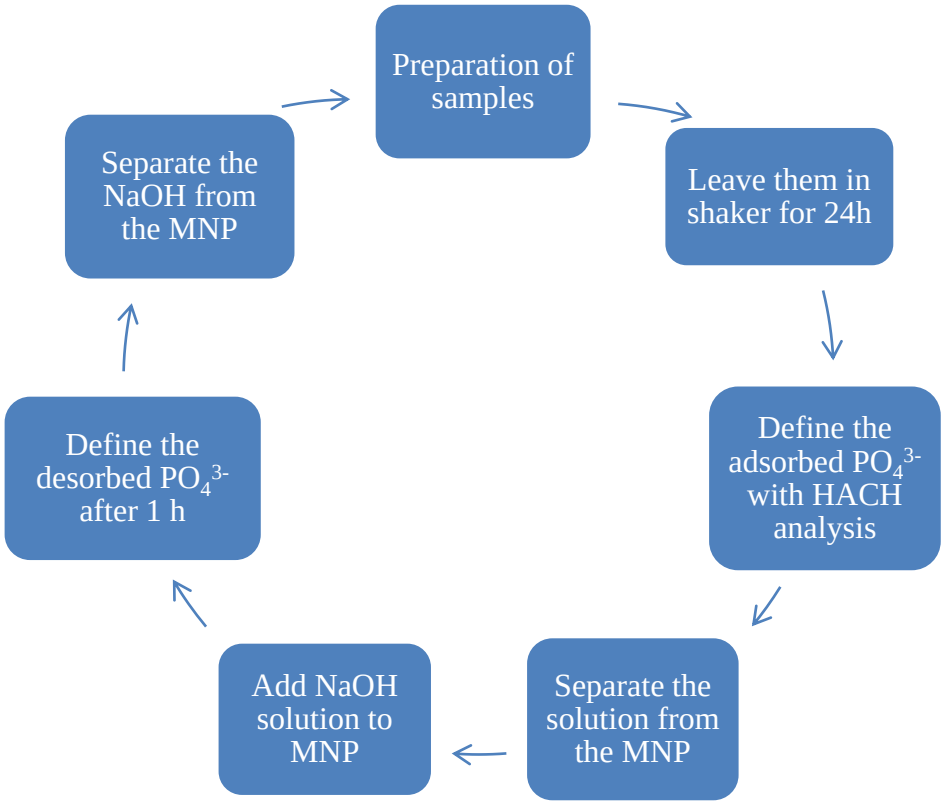

Figure 2.9. Flow diagram of desorption experiments

2.2.5. Analytical methods

The PO_4^{3-} concentration was measured with Amino Acid Method (Method 8178), which is a fast and accurate colorimetric measurement. The reaction between phosphate and reagents (1 mL Amino Acid Reagent and 1 mL Molybdate Reagent) causes a blue tint in the sample. The results will be displayed in mg/L (ppm) of phosphate (PO_4^{3-}). These reagents are designed to be used with samples that have an expected range of 0.0 to 30.0 mg/L phosphate. The phosphate concentrations were observed with HACH DR2500 Spectrophotometer on wavelength 880 nm.

For the characterization of supernatant solution and to determine the wastewater quality parameters Chemical Oxygen Demand (COD) was measured with colorimetric method with potassium dichromate ($K_2Cr_2O_7$) and sulfuric acid (H_2SO_4) on 600 nm in HACH spectrophotometer. The COD is the amount of oxygen consumed to chemically oxidize organic water contaminants to inorganic end products.

Ammonia was measured with direct Nesslerization Method with Mineral Stabilizer, Polyvinyl Alcohol and Nessler reagent, the yellow color shows the present of NH_3-N. The samples were tested in HACH spectrophotometer on 380nm.

2.2.6. Validation of kinetic and isotherm models

For the evaluation of kinetic and isotherm data we used Microsoft Office Excel software.

The acquired model was calculated according to Chi square (x^2), correlation coefficient (R^2) and normalized root mean square error (NRMSE). Table 2.2 shows the equations used for the calculation of these parameters.

Table 2.2. Validation parameters used for model evaluation

Parameter	Equation
Chi square	$x^2 = \sum_{i=1}^{n} \frac{(q_{exp} - q_{calc})^2}{q_{calc}}$
Correlation coefficient	$R^2 = 1 - \frac{\sum_{i=1}^{n}(q_{exp} - q_{calc})^2}{\sum_{i=1}^{n}(q_{exp} - q_{exp,mean})^2}$
Normalized root mean square error	$NRMSE = \frac{\sqrt{\frac{\sum_{i=1}^{n}(q_{exp} - q_{calc})^2}{n}}}{q_{exp,max} - q_{exp,min}}$

Where n is the number of data points; q_{exp} and q_{calc} are the quantities adsorbed determined experimentally and the quantities adsorbed calculated by the models, respectively; $q_{exp,max}$ and $q_{exp,min,}$ $q_{exp,mean}$ are the maximum, minimum and mean values of the quantities adsorbed determined experimentally, respectively.

3. Results and Discussion

3.1. Characterization of the adsorbent

The adsorbent material synthesized magnetic iron nanoparticles were characterized by Zeta potential analyzer, Fourier transform infrared (FTIR) spectroscopy, X-ray diffraction (XRD), scanning electron microscopy (SEM) and energy dispersive X-ray spectrometry (EDX).

3.1.1. Point of zero charge

This value helped us to set the most fitting pH value during the experiments.

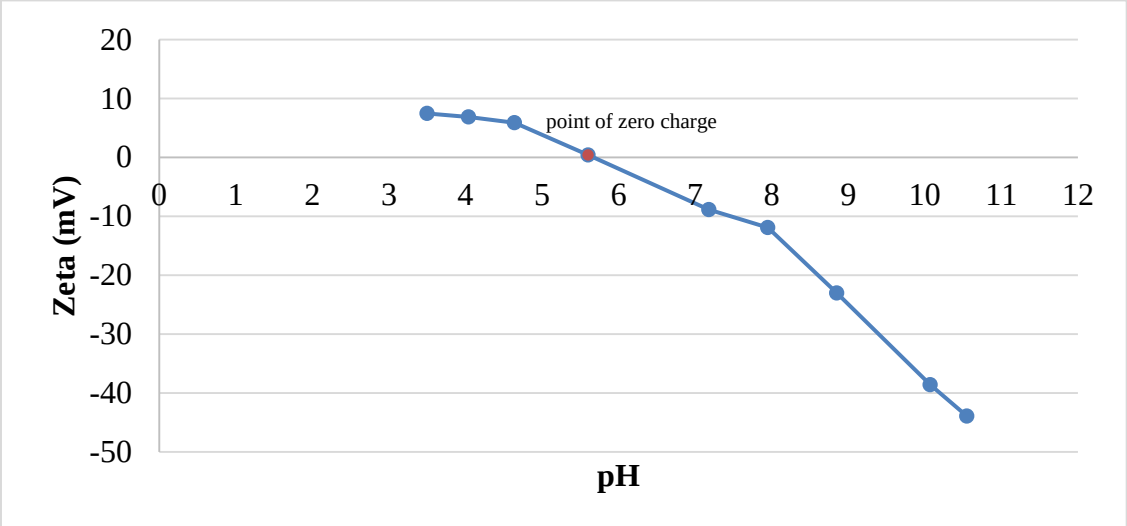

Figure 3.1. Zeta potential at different pH values

The zeta potential measurements as a function of pH (Figure 3.1) showed that the iron oxide surface charge is electropositive when pH values are lower than 5.6 and electronegative at pH values higher than 5.6. It means that the point of zero charge (pH_{zpc}) value was 5.6 for the produced MNP. The adsorption of the negatively charged phosphate ion to positively charged nanoparticles is favorable below pH_{pzc}. Because of the value of point of zero charge for experiments we set pH below 5.6.

3.1.2. FT-IR results

Fourier-transformed infrared spectroscopy results of pure magnetic iron oxide, after adsorption and after desorption with synthetic P solution is given in Figure 3.2.

In the FT-IR spectrum of raw MNP (Figure 3.2 (a), the peaks of 1326.8, 1552.4 and 3182.0 cm^{-1} indicated vibrations of functional group (Chen et. al., 2008; 2011) such as OH, and corresponded to the bending vibration of the H_2O molecules. Additionally, the peaks at 848.5 cm^{-1} corresponded to the Fe-OH vibration. There is a sharp peak at 540.0 cm^{-1} that is ascribable to Fe-O vibrations.

On the spectra of the MNP after the adsorption with synthetic P solution a few changes seen compared with the spectra of the pure MNP. Peak at 1326.8 cm^{-1} disappeared and 1003.8 cm^{-1} can be seen on the FTIR spectra after adsorption, this peak is attributed to the asymmetric stretch vibration of P-O of PO_4^{3-} group on MNP (Xu et al., 2017). P-O stretching bands encountered in PO_4^{3-} units are often identified in the range 990-1100 cm^{-1} (Salah et al., 2006). The characteristic adsorption bands of the Fe-O bond of magnetite were originally in 540.0 cm^{-1} and 451.3 cm^{-1}. This result was the evidence that the phosphorus was chemically bond to the surface of the magnetic iron oxide particles. After phosphate adsorption these bands shifted to 539.0 cm^{-1} and 455.1 cm^{-1} and they divide into smaller fractions. These diversions may sign that the interactions between phosphate and MNP are intermolecular origin (Maciel et al., 2012).

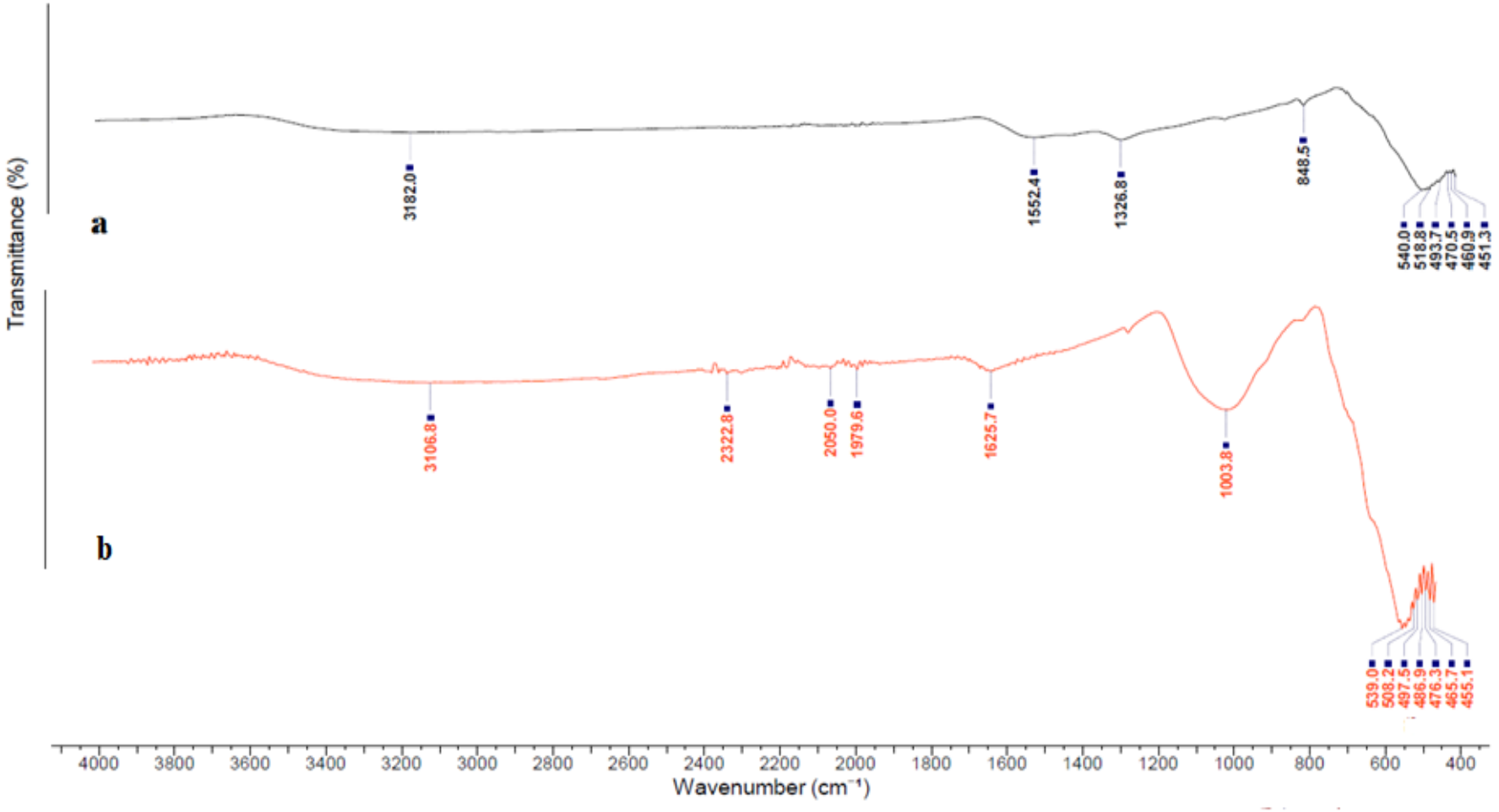

Figure 3.2. FTIR spectra of raw MNP (a) and MNP after adsorption with synthetic P solution (b)

On the following figure the FTIR analysis of pure MNP, after adsorption with $(NH_4)_2SO_4$ solution and after adsorption with supernatant is showed (Figure 3.3).

The FTIR analysis result of raw MNP was previously discussed for the interpretation of Figure 3.2.

The peak at 1621.8 cm^{-1} on Figure 3.3 (b) is more sharp than the peak at 1633.4 cm^{-1} with supernatant, which shows the stronger NH_4 bending vibration in NH_2.

FTIR spectrum of MNP after adsorption with supernatant shows that the adsorption was different than the MNP with synthetic P solution. After the evaluation of FTIR analysis of the adsorption with supernatant it was confirmed the MNP could adsorb the NH_3 too. To get a clearer picture about the meaning of the peaks, FTIR analysis of adsorbed NH_3 with $(NH_4)_2SO_4$ solution was done.
The peak at 1633.4 cm^{-1} shows NH_4 bending vibration in NH_2, the presence of a broad peak at the wave number 3218.6 cm^{-1} is attributed to the physical absorption of water molecules by N-H or O-H groups (Bautista et al., 2005). The peak at 1326.8 cm^{-1} in this case disappeared too, but a new peak appeared at 1012 cm^{-1}. The peak of 1012 shows FeOH groups, P-OFe vibration, P-O, it means that the phosphorus was chemically bond to the surface of the MNP. Ligand exchange mechanism was supported by FT-IR analysis.

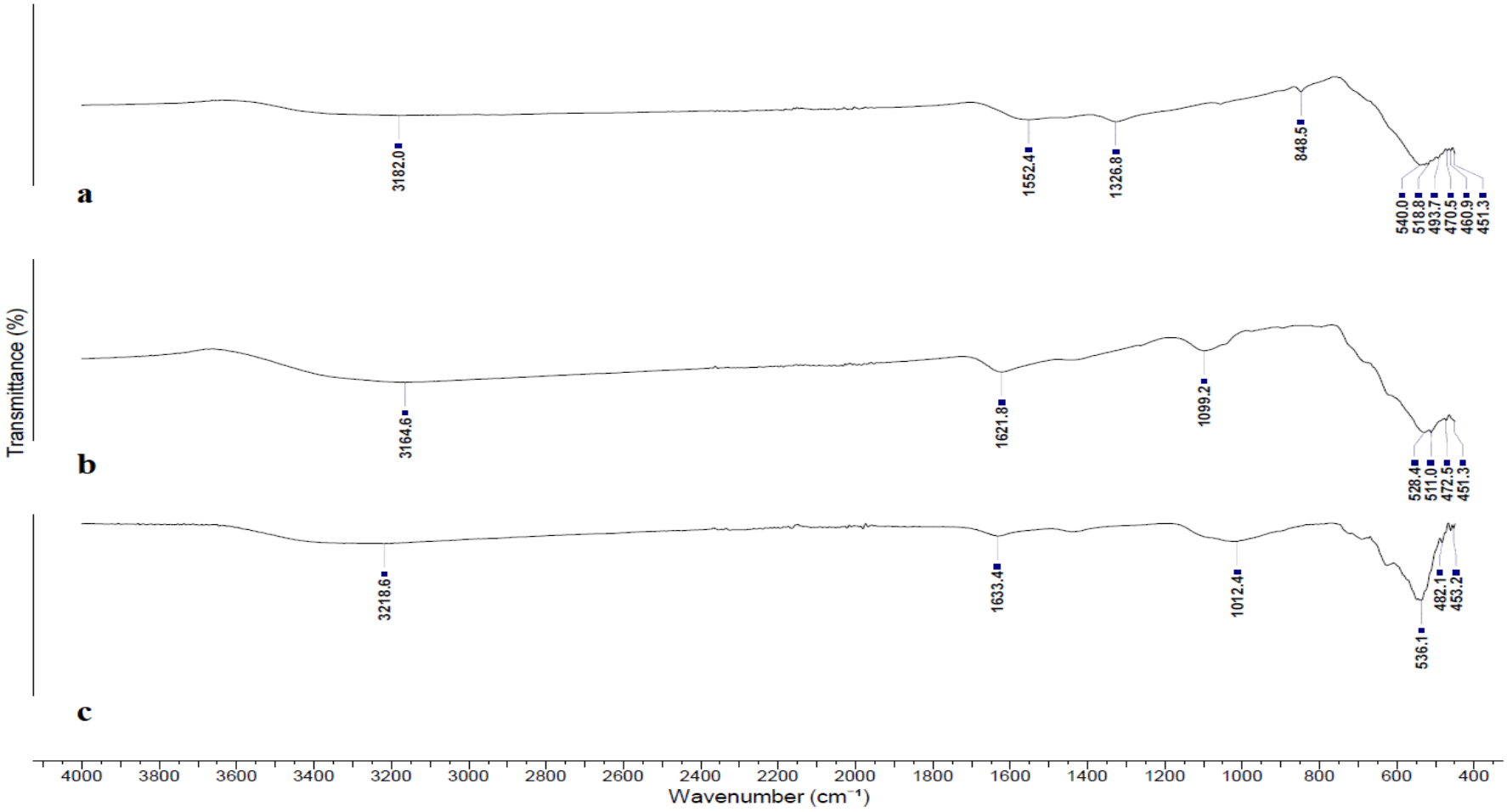

Figure 3.3. FTIR spectra of raw MNP (a), after adsorption of NH_3-N (b) and after adsorption with supernatant (c)

3.1.3. XRD results

The XRD analysis was employed to determine the structural construction and crystalline size of raw MNP (Figure 3.4).

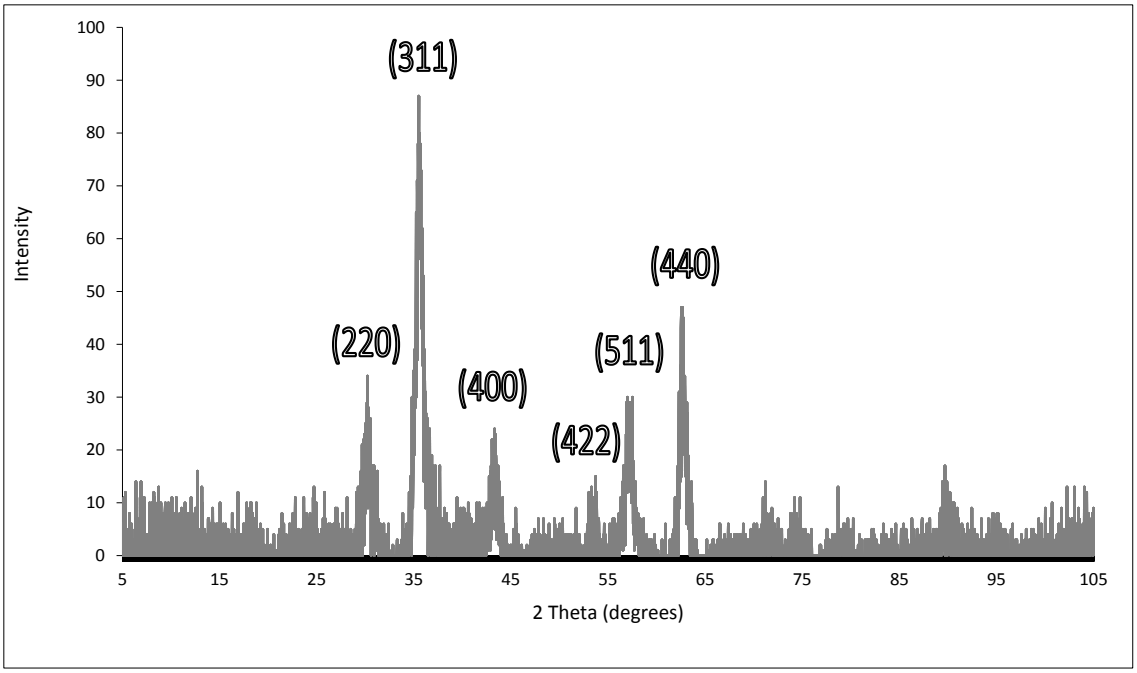

Figure 3.4. X-ray diffraction pattern of pure MNP

XRD patterns well determined that the crystal structure of iron oxide in the magnetite phase is matches with our synthesized magnetic nanoparticles. The main diffraction peaks (220, 311, 400, 422, 440 and 511) of raw MNP can be seen on Figure 3.4. The characteristic for Fe_3O_4 crystal phase is equivalent with the Joint Committee of Powder Diffraction Standards (JCPDS) database, which means they MNP was successfully synthesized.

The outcome of x-ray diffractometry additionally can be used to calculate the crystal size of the sample based on Scherrer (Scherrer, 1918) equation, described as:

$$\tau = \frac{K\lambda}{\beta \cos\theta} \tag{3.1}$$

where ι shows the size of the crystalline domains (nm), K is Scherrer constant (0.9), λ is the X-ray wavelength (Å), β is the half high width of the diffraction peak of the sample

(FWHM), and θ is the diffraction angle (°).

Using the previous equation with 0.154 nm wavelength for Cu-Kα radiation, the estimated crystalline size of MNP is 10.35 nm.

3.1.4. SEM results

For the characterization of the microstructure of the MNP after adsorption SEM analysis was used (Figure 3.5)

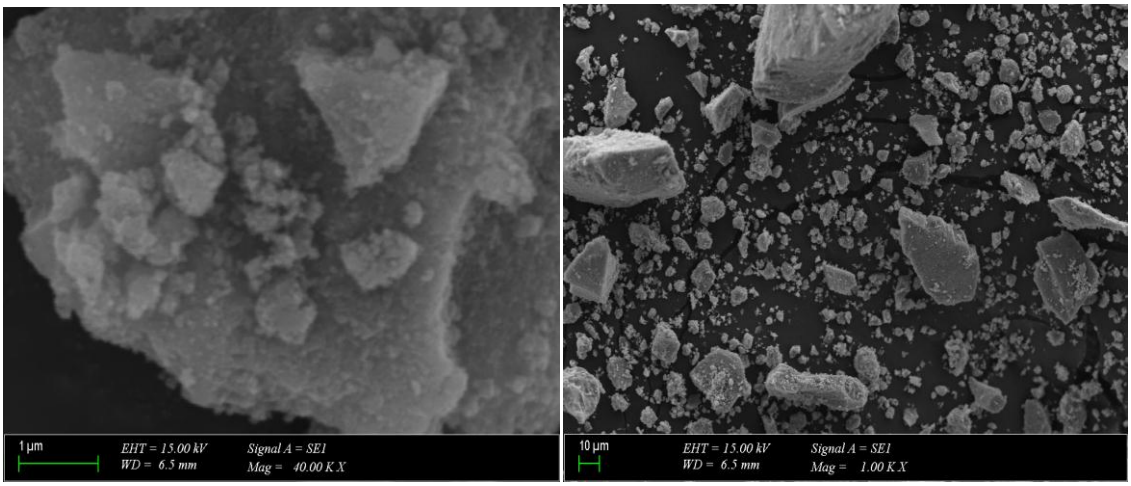

Figure 3.5. SEM images of MNP after adsorption

As the results shows on Figure 3.5 the adsorbent particles were nano sized, and the sizes were approximately 50 nm. The anomalistic shape of MNP has a rough surface was noticed, which was because of the use of crushed MNP. The particles in the synthetic magnetite samples are in most cases aggregates, and it is proved by our SEM analysis too (Sun et al., 1998). Because of the agglomeration of nanoparticles, the surface area and number of surface reaction sites can be reduced. Moreover, the intraparticles diffusion distance is increased and the result of it the adsorption capacity is reduced as well (Lai et al., 2016).

SEM results were evaluated according to JUPAC classification of porous solids, and it is the following; macroporous> 50 nm, mesoporous 2-50 nm and microporous < 2 nm.

According to JUPAC classification all samples have highly porous structure and mostly macroporous (pores have diameters higher than 50 nm). Moreover in the samples we

can find pores with diameters between 2-50 nm, and it shows the existence of meso-phores.

3.1.5. EDX results

Figure 3.6 shows the elements founds on the surface of MNP after adsorption according to their weight percentage.

EDX analyses were carried out to prove the adsorption of P and N elements.

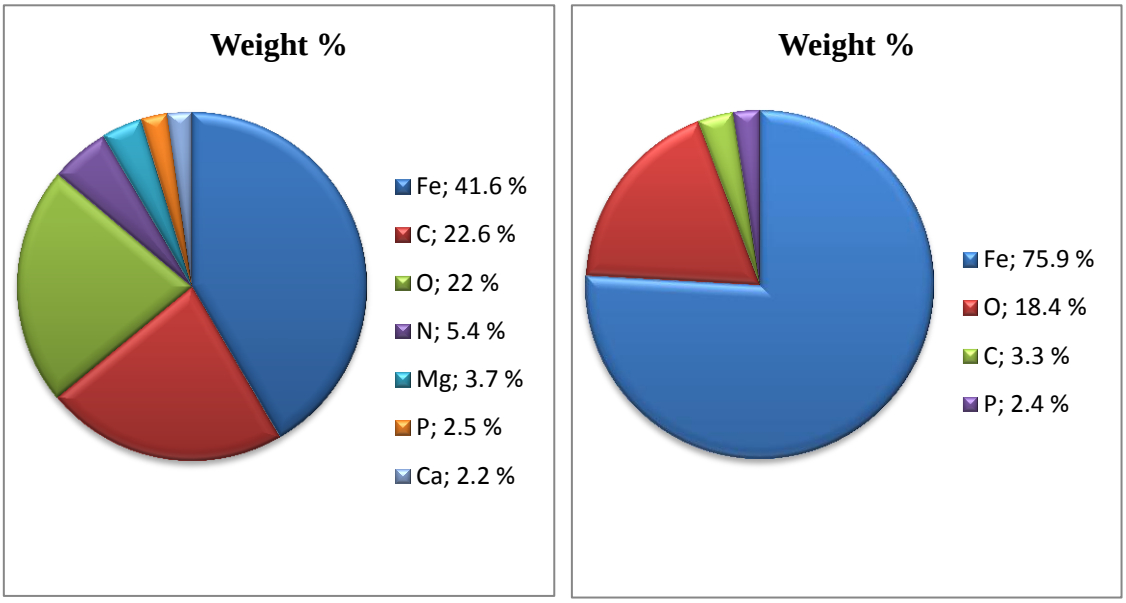

Figure 3.6. EDX after adsorption of PO_4^{3-} from supernatant (left) and synthetic P (right) solutions.

According to EDX results after adsorption with supernatant (Figure 3.6 left), we can confirm that the MNP is capable of the adsorption of P, C, moreover N, Ca and Mg.

3.2.Adsorption performance

3.2.1. Effect of P concentration – equilibrium tests

The initial P concentrations were varied from 29 to 1046 mg/L, adsorbent dosage was 15 g/L, and the reaction time was 24 h with ~3 as initial pH.

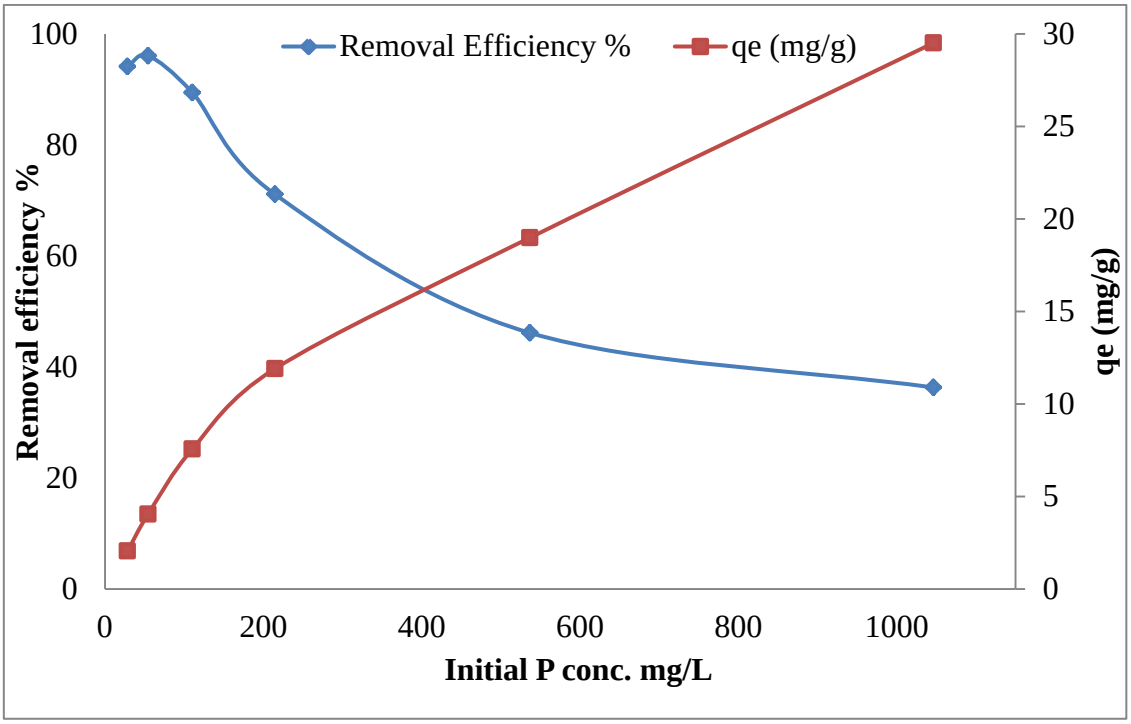

Figure 3.7. Effect of initial phosphate concentration (dosage of adsorbent: 15 g/L; initial P concentrations: 54-1046 mg/L; pH: ~ 3; 24 h; 25 °C)

As Figure 3.7 shows the P concentration increased and the removal efficiency decreased from ~ 96 % (with 54 mg/L initial P concentration) to ~ 31 % (with 1046 mg/L initial P concentration), because the limitation of surface area and the MNP had no more capability to adsorb additional phosphorus. The highest and lowest equilibrium adsorption capacities were 29.5 mg/g and 2.1 mg/g, respectively.

To analyze the equilibrium data for the adsorption of MNP, two parameter (Freundlich and Langmuir) and three parameter isotherm models (Sips, Redlich-Peterson) were tested.

The Freundlich isotherm (Freundlich, 1907) is applicable for non-ideal adsorption on heterogeneous surfaces with multi-layer sorption and it's expressed as:

$$q_e = K_F C_e^{1/n} \quad (3.2)$$

where q_e is the equilibrium adsorption amount (mg/L) at equilibrium concentration of C_e (mg/L), K_F is Freundlich coefficient characteristic of the adsorption affinity, related

to the adsorption capacity of the adsorbent ((mg/g)/(mg/L)$^{1/n}$) and 1/n is the Freundlich intensity parameter (Davila et. al., 2005).

The other tested isotherm in this study is the Langmuir model (Langmuir et.al., 1918). This isotherm can describe monolayer adsorption on homogeneous surface as;

$$q_e = \frac{Q^0_{max} K_L C_e}{1 + K_L C_e} \tag{3.3}$$

where q_e is the equilibrium adsorption amount (mg/g) at equilibrium concentration of C_e (mg/L), K_L is Langmuir constant and Q^0_{max} is the maximum adsorption capacity calculated from Langmuir model.

The Sips isotherms (Sips, 1948) in an empirical model which combines the ability of Langmuir and Freundlich isotherms. In pursuance of this model, the surface of the sorbent can be homo- or heterogeneous.

$$q_e = \frac{q^S_m K_S C_e^{1/n_S}}{1 + K_S C_e^{1/n_S}} \tag{3.4}$$

where q_e is the equilibrium adsorption amount (mg/g) at equilibrium concentration of $C_e^{1/nS}$ (mg/L), K is the Sips equilibrium constant, $1/n_S$ is the Sips heterogeneity constant and q_{max}^S is the maximum adsorption capacity calculated from Sips model.

Redlich and Peterson (Su et. al., 2012) proposed an empirical equation, which can be used to represent adsorption equilibria over a wide concentration range:

$$q_e = \frac{K_R C_e}{1 + a\, C_e^b} \tag{3.5}$$

where K_R and b are Redlich-Peterson constants and C_e is equilibrium concentration. The ratio of K_R/a_R indicates the adsorption capacity, it is applicable in either homogenous or heterogeneous systems because of its versatility.

Table 3.1. Equilibrium adsorption isotherms' parameters

Model	Model parameters	Goodness of fit measures
Langmuir	Q_{max} (mg/g) = 20.825 K_L (L/mg) = 0.0279	R^2 = 0.936 x^2 = 4.782 NRMSE = 0.04
Freundlich	K_F ((mg/g)/(mg/L)$^{1/n}$) = 0.314 $1/n_K$ = 2.823	R^2 = 0.979 x^2 = 1.3 NRMSE = 0.0518
Sips	q^s_m (mg/g) = 34.161 K_s (mg/L) = 0.0629 $1/n_s$ = 0.4988	R^2 = 0.988 x^2 = 0.757 NRMSE = 0.0106
Redlich- Peterson	K_R (mg/L) = 2.179 a = 0.453 b = 0.769	R^2 = 0.992 x^2 = 0.64 NRMSE = 0.032

Table 3.1 shows that determination coefficient (R^2) value was comparatively higher at the Redlich-Peterson isotherm, because this it is the most suitable to represent our results in the test with phosphate solution by MNP, with high R^2 (0.992), high x^2 (0.64) and NRMSE (0.032).

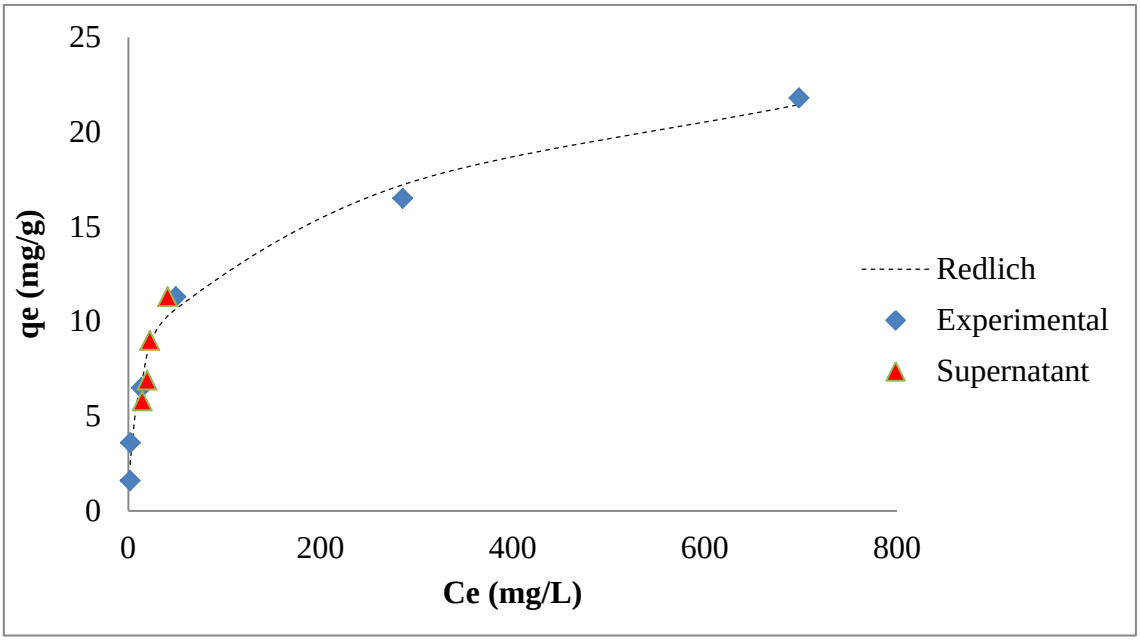

Figure 3.8. Redlich-Peterson isotherm model for synthetic phosphate solution and supernatant concentration (dosage of adsorbent: 15 g/L; initial P concentrations for synthetic P solution: 54-1046 mg/L; pH: ~3; for supernatant solution: 166 mg/L; pH: ~ 5; 24 h; 25 °C)

Synthetic P solution and supernatant solution was consistent with the Redlich-Peterson isotherm. The difference between the results is the maximum adsorption capacity (q^{s}_{max}). This value is significantly bigger at the P solution, because of higher initial P concentrations.

In Table 3.2 the maximum adsorption capacities of the previous studies are given, which use similar experimental conditions (pH and °C).

Table 3.2. Comparison of phosphate adsorption capacity of MNP

Adsorbent title	Adsorption capacity (mg/g)	pH	°C	Reference
Magnetite	3.65	2.77	44.85	Tu et al., 2015

Fe_3O_4/ZrO_2/chitosan composite	26.5	3	25	Jiang et al., 2013
MIO	15.2	4	25	Choi et al., 2016
MIO	5.03	-	30	Yoon et al., 2014
Magnetite	27.15	~7	25	Vicente et al., 2010
Magnetite	20.83	~3	25	This study

3.2.2. Kinetic analysis

Kinetic models are used to evaluate the performance of the adsorbent for the removal of target phosphorus for aqueous solutions. Three avowed kinetic models, the pseudo-first order (PFO), the pseudo-second order (PSO) and the Elovich models have been tested in this study.

Lagergren's equation (Lagergren, 1898), the pseudo-first order equation is described as:

$$q_t = q_e\,(1 - e^{-k_1 t}) \tag{3.6}$$

where, q_t and q_e are the amounts of phosphorus adsorbed (mg/g7) at time, t (min) and at equilibrium, k_1 is the rate constant of PFO equation (1/min).
Pseudo-second order is given as:

$$q_t = \frac{q_e^2 k_2 t}{1+q_e k_2 t} \tag{3.7}$$

where, q_t and q_e are the amounts of phosphorus adsorbed (mg/g) at time, t (min) and at equilibrium, k_2 is the rate constant of PSO equation (g/mg min).

Elovich equation is shown as the following equation:

$$q_t = \frac{1}{\beta}\ln(1 + \alpha\beta t) \quad (3.8)$$

where, q_t is the amount of phosphorus adsorbed (mg/g) at time, t (min); α and β are constants.

Kinetic and equilibrium adsorption measurements have essential role to get information for the design and operation of phosphate removal process in water/wastewater treatment (Yuchi, 2014).

In kinetic measurements both synthetic P solution (initial P concentration 554 mg/L) and supernatant (initial P concentration 166 mg/L) solution were used, varied reaction time was tested from 1 to 1440 min.

Table 3.3. Evaluation of kinetic models for P adsorption by MNP with P solution

Model	Model constant	R^2	x^2	NRMSE
PFO	k_1 = 0.0604 min^{-1}	0.397	141.866	0.628
PSO	k_2 = 0.0778 g/(mg·min)	0.637	5.661	0.499
Elovich	α = 22559.55 mg/(g·min) β = 1.06 g/mg	0.924	1.343	0.066

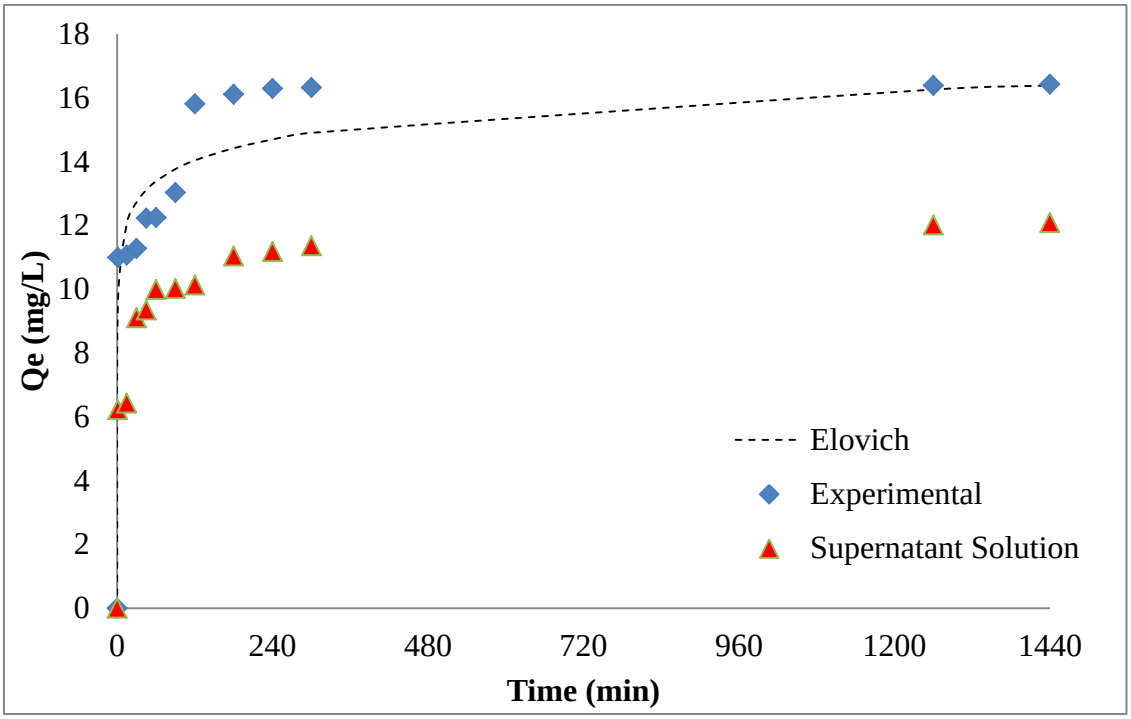

Figure 3.9. Elovich kinetic model of synthetic P solution and supernatant adsorption (dosage of adsorbent: 15 g/L; initial P concentrations for synthetic P solution: 554 mg/L; pH: ~3; for supernatant solution: 166 mg/L; pH: ~ 5: 1-1440 min; 25 °C)

The P adsorption trend profile is similar (Figure 3.9) and both synthetic P and supernatant solution was consistent with Elovich kinetic model. The difference is the lower equilibrium P concentration of the supernatant solution, because of the initial P concentration is lower too.

The adsorption with synthetic P solution the PO_4^{3-} is quickly adsorbed in the first 90 minutes. The P adsorption rate increased with time till the measurement at the 120th minute, after that time period it became almost steady. Equilibrium P amount was achieved to be 16.11 mg/g. The phosphate concentration decreased progressively with increasing contact time until equilibrium was reached. The phosphate concentration decreased to 326 mg/L at 120 min of contact time and further decreased to 317 mg/L at 24 h. The phosphate sorption reached equilibrium at 2 h of reaction time with a phosphate concentration of 326 mg/L. The sorption capacity increased from 11 to 16.4 mg/g with increasing reaction time from 1 to 1440 min. With initial phosphorus concentration of about 554 mg/L, the concentration after treatment can achieve nearly 317 mg/L

(about 43 % of removal efficiency). The efficiency increased quickly in 120 minutes after started shaking and began slowly until reached saturated. Removal efficiency of about more than 40 % can be reached after 120 minutes.

When the supernatant was the aqueous solution, after a fast adsorption period occurred for 1–30 min, the adsorption of the measured phosphate slowed down. Equilibrium was achieved to be ~12 mg/g. The results show that the phosphate adsorbed amount increased with increasing contact time until equilibrium was reached. The phosphate concentration decreased to 49 mg/L at 30 min of contact time and further decreased to 10 mg/L at 24 h. The phosphate sorption reached equilibrium at 5 h of contact time with a phosphate concentration of 19 mg/L. The adsorption capacity increased from 6.22 to 12.09 mg/g with longer reaction time from 1 to 1440 min. With initial phosphorus concentration of about 167 mg/L, the concentration after treatment can achieve nearly 10 mg/L (about 94 % of removal efficiency). The efficiency increased swiftly in 30 minutes after started shaking and slowed down until reached saturated. Removal efficiency of about more than 70 % can be reached after 30 minutes.

This result (Figure 3.9) shows the competence of MNP in phosphate sorption at a short reaction time to reach equilibrium.

3.2.3. Effect of adsorbent dosage

The effect of adsorbent dosage on phosphorus adsorption was examined with supernatant solution by varying the adsorbent dosage from 10 to 25 g/L with an initial P concentration of 136 mg/L. The importance of the MNP concentration is showed on Figure 3.10.

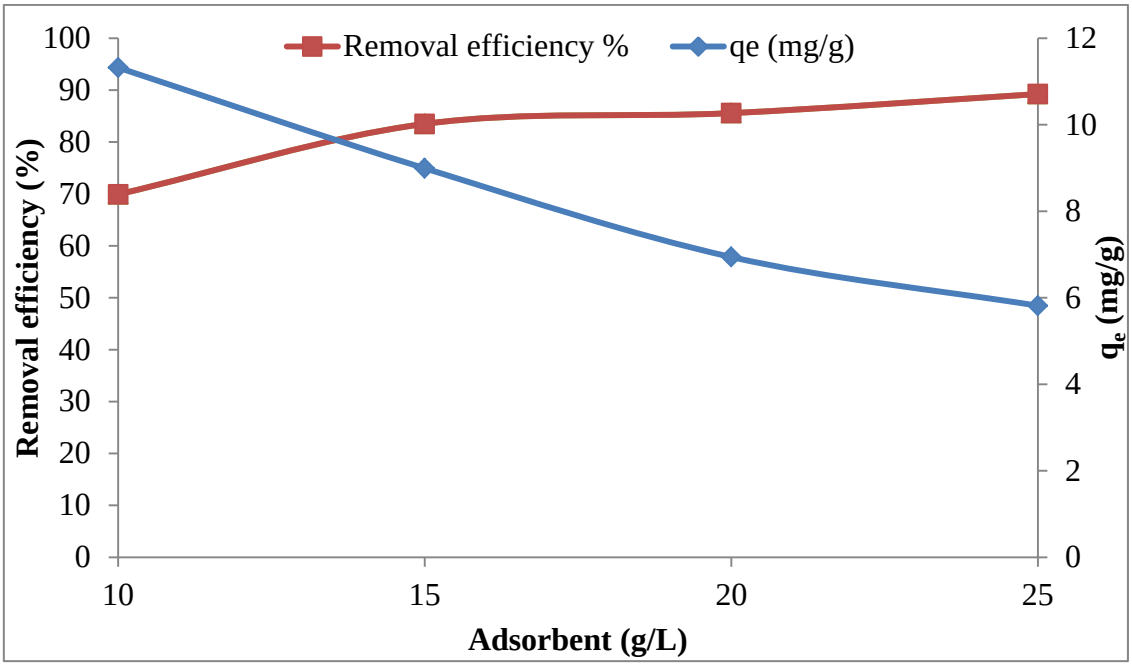

Figure 3.10. Phosphate removal efficiency by MNP and adsorption capacity as a function of adsorbent dose (dosage of adsorbent: 10-25 g/L; initial P concentrations: 136 mg/L; pH: ~3; 24 h; 25 °C)

The removal efficiency of P in supernatant solution increased with the increase of adsorbent dosage (Figure 3.10). The adsorbed P increased from 69.9 % at 10 g/L adsorbent dosage to the maximum removal of 89 % at 25 g/L adsorbent dosage. The growth in the phosphate adsorption with the increase in the adsorbent dosage can be associated with the increase in magnetic iron oxide adsorbent's surface adsorption site. However results show there is just 5 % difference - in removal efficiency -, between adsorbent dose of 15 g/L and 25 g/L. It means there is no need for extra surface capacity because of the low initial P concentration, and the optimum dosage is 15 g/L.

The adsorption capacity decreased with increasing adsorbent dose, at 10 g/L the sorption capacity was 11.3 mg/g and decreased to 9 mg/g at 15 g/L. The adsorption capacity decreased to 6.9 mg/g at 20 g/L and decreased further to 5.8 mg/g at 25 g/L.

3.2.4. Effect of pH

The effect of pH on phosphate adsorption was examined with supernatant solution (initial P ~166 mg/L; 0.3 g adsorbent). This experiment was important, to see how adsorption capacity changes, when pH of the supernatant solution is not adjusted. pH adjust-

ment requires chemicals, which can be expensive, this is why we compared adjusted (initial ph ~5) and non-adjusted (initial pH 8.1) pH (Figure 3.11).

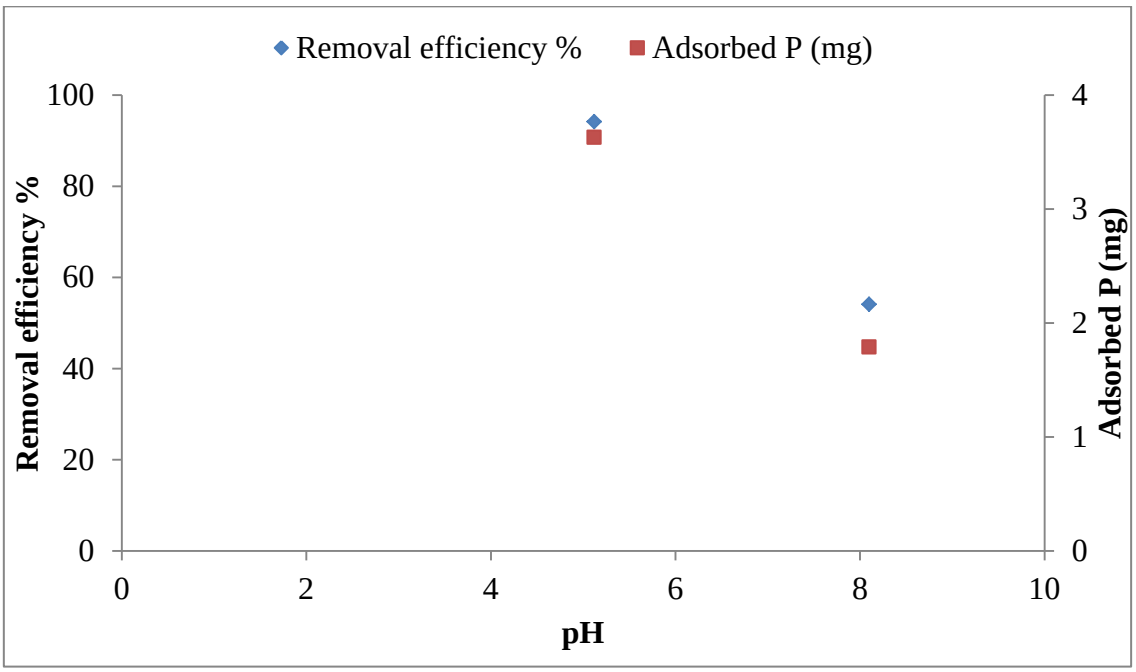

Figure 3.11. Removal efficiency with different initial pH (dosage of adsorbent: 15 g/L; initial P concentrations: 166 mg/L; pH: ~ 5, ~8; 24 h; 25 °C)

The removal efficiency at pH ~5 was 94 % and at pH ~8 it decreased to 54 %. There is steady decrease of the amount of adsorbed phosphate from 3.63 to 1.79 mg/g as pH increased from ~5 to ~8; this might be caused by electrostatic attraction. At higher pH, the phosphate adsorption capacity is reduced because of the strong competition between P species ($H_2PO_4^-$, HPO_4^{2-} and PO_4^{3-}) and hydroxyl (OH^-) ions on the adsorbent surface (Ajmal et al., 2018; Jung et al., 2015; Lalley et al., 2016).

3.2.4.1.Adsorption of NH_4-N

For examination of the NH_4-N adsorption capacity of MNP was tested on supernatant solution and NH_4 solution after adsorption.

During supernatant adsorption experiments NH_4-N values were measured. Initial NH_4-N concentration of supernatant was 740 mg/L, at this measurement initial pH was ~5. Table 3.4 shows the final NH_4-N concentrations after adsorption, with different MNP dosage.

Table 3.4. NH_4-N concentrations of supernatant after adsorption

MNP dosage (g/L)	Final NH_4-N concentration (mg/L)
10	560
15	520
20	580
25	660

Additionally NH_4 solution was tested with initial NH_4-N concentration 1280 mg/L, adsorbent dosage of 15 g/L and with different initial pH (Table 3.5).

Table 3.5. Adsorption results of NH_4 solution

pH	Final NH_4-N concentration (mg/L)
8.4 (pH adjustment was not done)	1170
3	1100

These tests (Figure 3.4 and 3.5) confirm that the MNP is able for the adsorption of the NH_4-N.

3.3.Desorption experiments

Batch desorption tests were carried out to examine the recovery of phosphate with MNP. Desorption experiments were done with synthetic P solution and supernatant, too. A lot of studies (de Vicente et al., 2010; Tu and You, 2014; Zach-Maor et al., 2011b) proved that the NaOH solution is the most effective on desorbing P from magnetic iron oxide, by reason of this NaOH solution was used for desorption in our tests. Jeongyun et al. (2016), presented that the other alternative solution for desorption the NaCl can be, but their study described that the NaOH solution is more effective (Jeongyun et al., 2016).

For the desorption experiment the previously fully adsorbed MNP was used in an alkaline solution (NaOH ph ~12). The used magnetic nanoparticles dosage was the same as what we used for adsorption experiments; with P solution 0.3 g and with supernatant 0.2, 0.3, 0.4 and 0.5 g.

In each cycle 20 mL of NaOH was added during desorption tests and shaked for 1 hour at room temperature. In desorption experiments we reused the NaOH in each cycle, just

1-5 mL was added. The adsorption performance was tested in each cycle, in total 9-9 adsorption-desorption test had been made with synthetic P solution and 5-5 with supernatant solution.

The initial P concentration of synthetic P solution was ~520 and 1100 mg/L and the amount of adsorbent was 15 g/L.

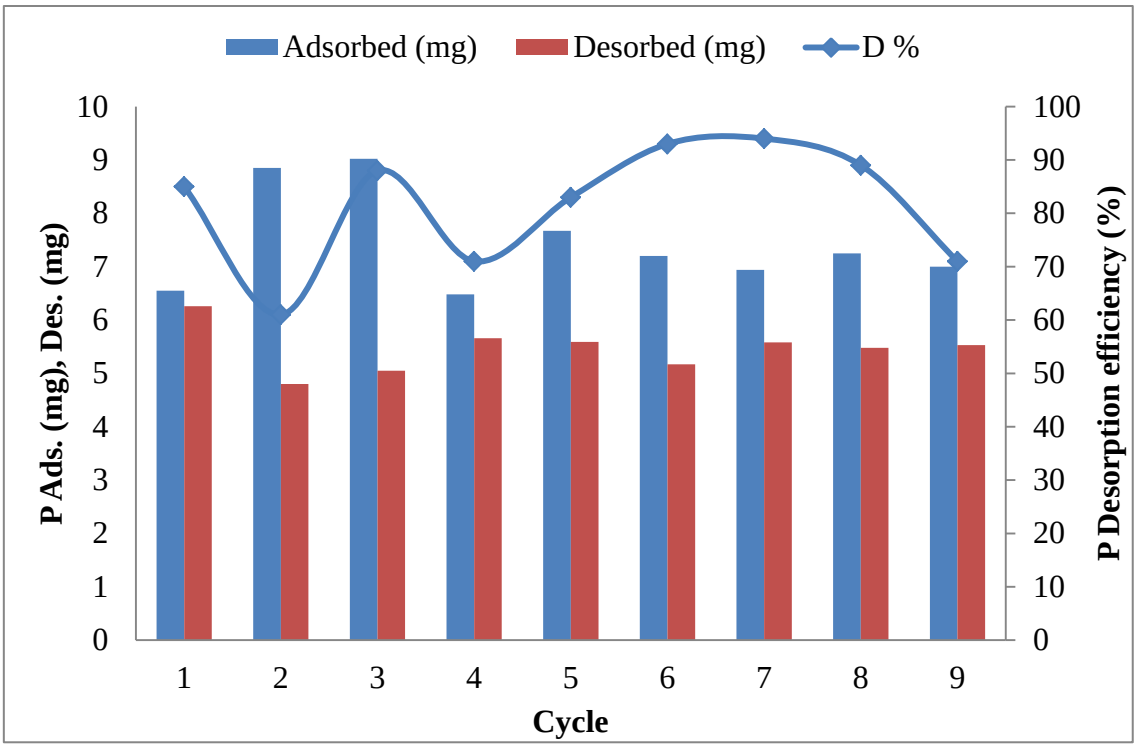

Figure 3.12. Efficiency of PO_4-P adsorption/ desorption in each cycles (500 mg/L) (dosage of adsorbent: 15 g/L; initial pH: ~3; 24 h; 25 °C)

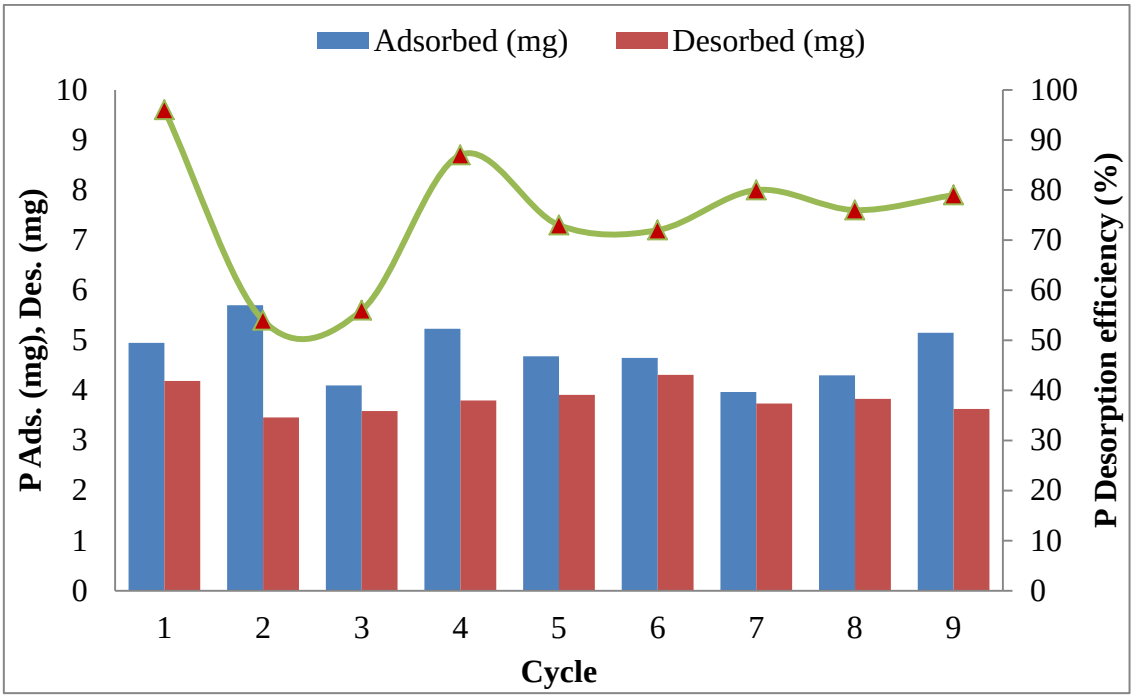

Figure 3.13. Efficiency of PO_4-P adsorption/ desorption in each cycles (1000 mg/L) (dosage of adsorbent: 15 g/L; initial pH: ~3; 24 h; 25 °C)

Figure 3.12 shows the synthetic phosphate solution's nine adsorption/ desorption cycle, with 520 mg/L, and the highest desorption capacity 94 %, in average it was 81.6%. Figure 3.13 shows the phosphate solution's nine adsorption/ desorption cycle, with 1100 mg/L, and in this case the maximum desorption capacity 96 %, in average it was 74.7%. The biggest desorbed amount was 6.26 mg with 520 mg/L and 4.31 mg with 1100 mg/L in one hour.

With supernatant we examined 5-5 adsorption/desorption cycle, with 10, 15, 20 and 25 g/L adsorbent amount and initial P concentration was ~140 mg/L. These tests were carried out to confirm the optimum adsorbent dosage.

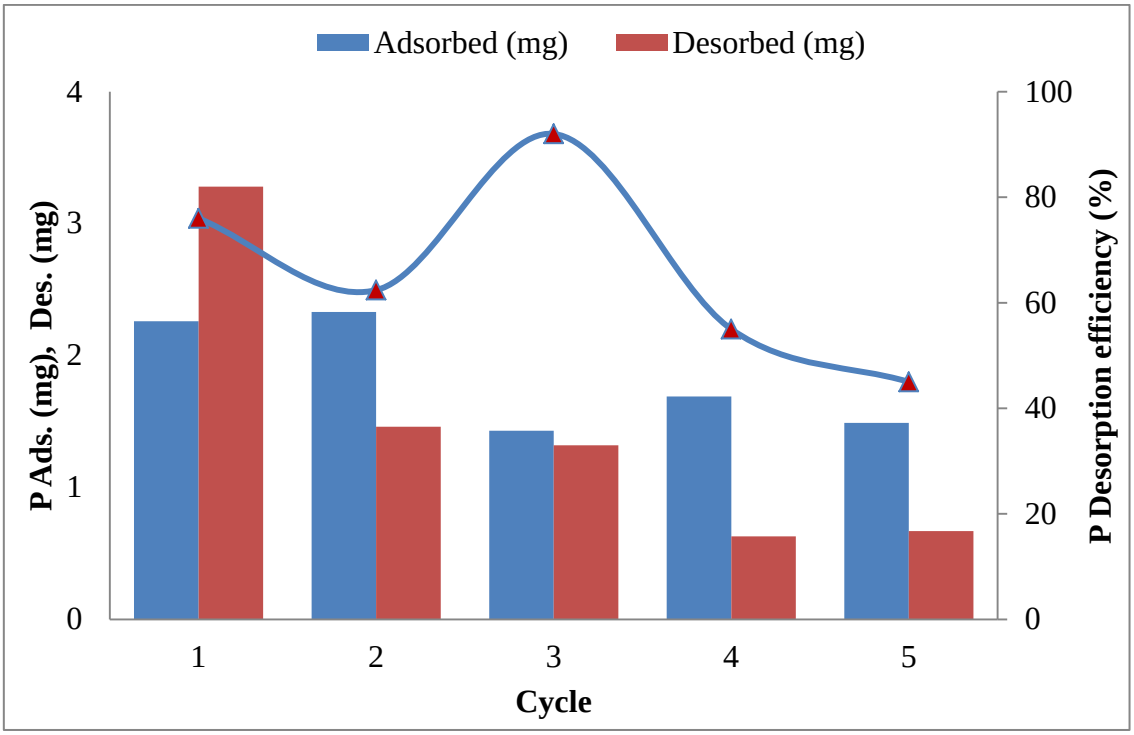

Figure 3.14. Efficiency of PO_4-P adsorption/ desorption in each cycles (10 g/L MNP) **(**initial P concentrations: 140 mg/L; initial pH: ~5; 24h; 25 °C)

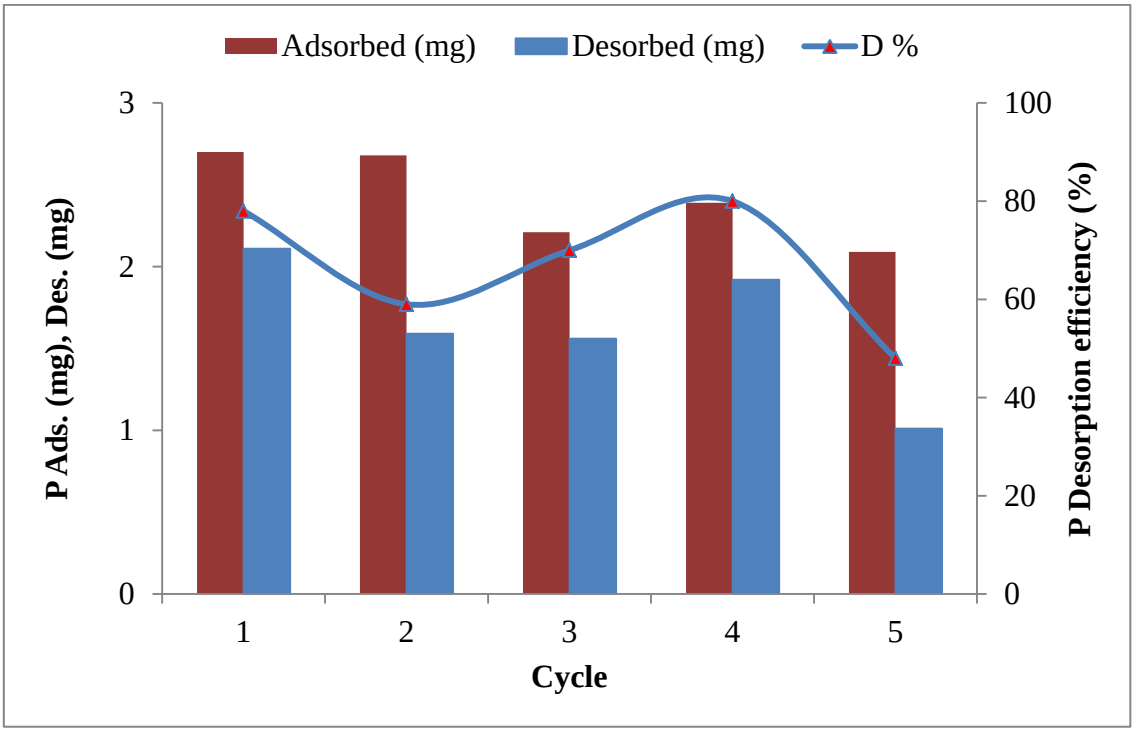

Figure 3.15. Efficiency of PO_4-P adsorption/ desorption in each cycles (15 g/L MNP) **(**initial P concentrations: 140 mg/L; initial pH: ~5; 24h; 25 °C)

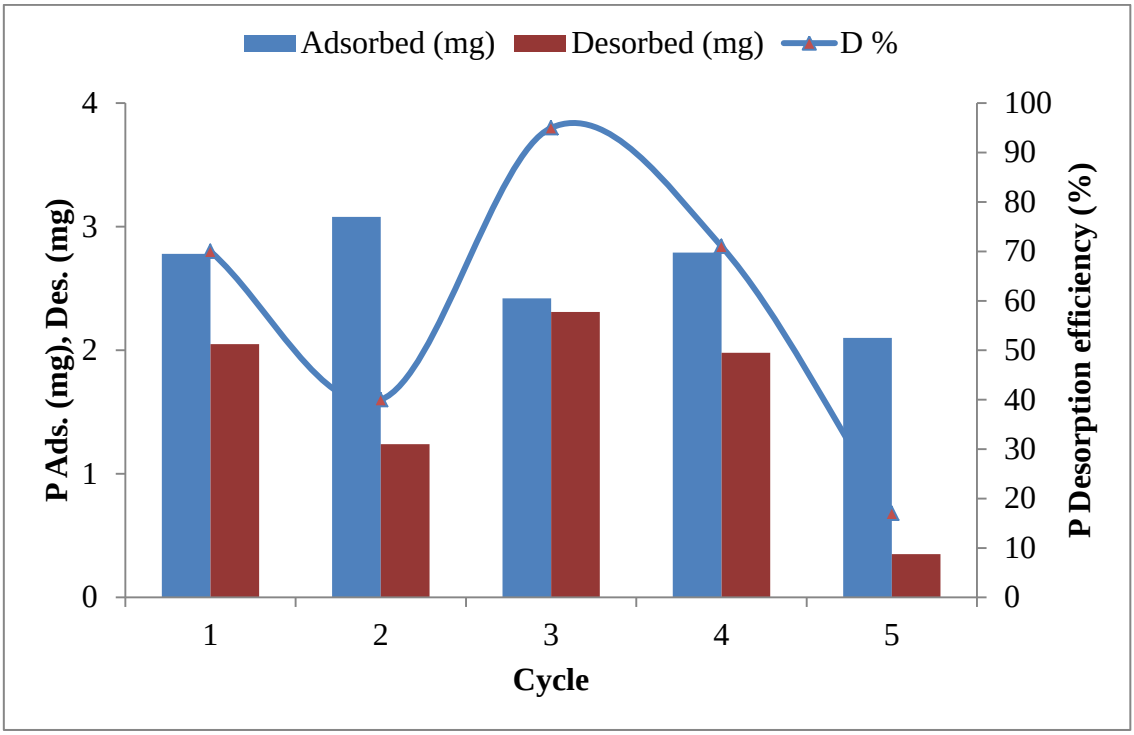

Figure 3.16. Efficiency of PO_4-P adsorption/ desorption in each cycles (20 g/L MNP) **(**initial P concentrations: 140 mg/L; initial pH: ~5; 24h; 25 °C)

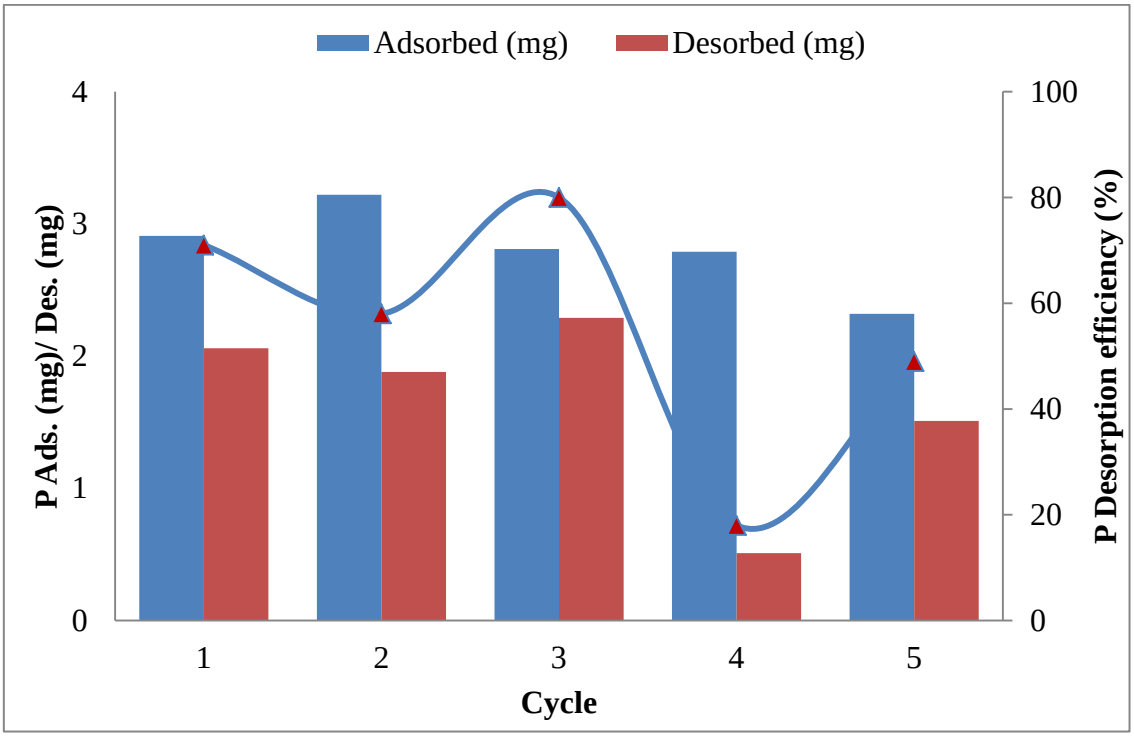

Figure 3.17. Efficiency of PO_4-P adsorption/ desorption in each cycles (25 g/L MNP) **(**initial P concentrations: 140 mg/L; initial pH: ~5; 24h; 25 °C)

Figure 3.14, 3.15, 3.16 and 3.17 shows the five adsorption/ desorption cycle of the supernatant with different adsorbent dosages. When the adsorbent dose was 10 g/L the highest desorption capacity was at the 4. cycle (Figure 3.14). With 15 g/L adsorbent dosage the desorption efficiency was 80 %, the tests with this amount of adsorbent dose showed the highest average desorption efficiency (67%) (Figure 3.15). Figure 3.16 shows that the most effective desorption was carried out with 20 g/L, in the third cycle of the experiment. The least effective desorption is shown on Figure 3.17 with 25 g/L MNP. The highest desorbed amount of P was 3.28 mg with 10 g/L in the first cycle.

These results confirm that the optimum MNP dosage can be 15 g/L for desorption of P with supernatant (initial P concentration 140 mg/L).

3.3.1. Desorption of NH_4-N

The NaOH solution, which was used at desorption experiments was tested for Mg and Ca ions after cycle 5 but there was no sign of these ions. The reason can be that the NaOH solution has no ability for the desorption of the NH_3.

The other additional experiment was the measurement of NH_4-N after desorption of supernatant. The initial NH_4-N concentration of supernatant was 590 mg/L. Table 3.6 shows the NH_4-N amount in the NaOH solution which was used for desorption with different adsorbent dosages (0.2, 0.3, 0.4 and 0.5 g).

Table 3.6. NH_4-N concentrations in NaOH solution after 5 adsorption-desorption cycles

MNP (g/L)	NH_4-N (mg/L)
10	200
15	320
20	110
25	90

According to these results, it is proved that the magnetic nanomaterial is capable for the adsorption of NH_4-N, too.

4. Conclusions

In this study, the adsorption, desorption and reusability of phosphate was examined from sewage sludge supernatant. For this reason magnetic iron oxide nanoparticles were used in various conditions.

The result of FT-IR, XRD and SEM tests showed that the magnetic nanoparticles were produced successfully and declarable that the phosphate unites with the MNP via electrostatic attraction, as a result forming a new outer sphere surface complex and inner-sphere surface complex under acidic condition.

XRD analysis showed that the chrystalline size of the MNP is 10.34 nm

FT-IR analysis results show the interaction between the MNP and P, moreover a MNP and NH_4.

On FTIR and EDX analyses showed that the magnetic nanomaterial is able for the adsorption of both phosphate and ammonium too.

Batch studies were used to accomplish the adsorption and desorption tests, with P solution and supernatant too.

For evaluation of the equilibrium tests, different isotherm models were used, the most consistent was the Redlich-Peterson isotherm. The maximum amount of phosphate adsorbed per unit weight of adsorbent was 20.83 mg/g according to Langmuir isotherm and 34.16 due to Sips model, for pure magnetic nanoparticles.

Kinetic studies showed that in the test with P solution and supernatant solution phosphate adsorption followed Elovich kinetic model. This experiment was carried out for the declaration of optimum reaction time. The test results showed that the MNP is able for the high percentage of adsorption in 2 hours contact time.

Furthermore due to the tests with different initial pH, it has effect on adsorption capacity as well, which was visible in a test with the supernatant. When the pH was adjusted to ~5 the removal efficiency was 94 %, at pH ~8 adjustment was not done and the removal efficiency decreased to 54 %. In the study of Nguyen et al. (2014) the same result was reported, they found with the changing surface properties the type of phosphate changing too and this is the main cause for decreasing phosphate removal efficiency with increasing pH (Nguyen et al., 2014). At different pH, different dominant phosphate species can be found and the forms of these species depend on the ionization constants

of phosphoric acid. At pH 7.5 phosphorous mainly can be found in the form of $H_2PO_4^-$, at pH 12 the dominant form is HPO_4^{2-} (Li et al., 2016a, 2016b).

Different adsorbent dosages were tested, and it is seen the optimum adsorbent dosage was 15 g/L on synthetic P solution and on supernatant solution, too.

Desorption tests were carried out as nine adsorption/desorption experiment on synthetic P solution and 5-5 on supernatant solution. According to the results, the maximum phosphorous desorption was 96 %, when the initial P solution was ~500 mg/L.

The highest average P desorption efficiency with supernatant solution was 67 % (15 g/L of MNP). Desorption experiments proved that the MNP can be reused several times.

This study presented that the magnetic iron oxide nanoparticle is a great sorbent for phosphate from aqueous solutions with desorption and reuse.

REFERENCES

Ábraham, A. (2016) Karbonsavval módosított magnetit nanorészecskék előállítása és vizsgálata, Bachelor Thesis, Eötvös Loránd Tudományegyetem, Budapest, Hungary, 3-14.

Ajmal, Z., Muhmood, A., Usman, M., Kizito, S., Lu, X., Dong, R., Wu, S. (2018) Phosphate removal from aqueous soultion using iron oxides: Adsorption, desorption and regeneration characteristics, Journal of Colloid and Interface Science 538, 145-155

Arai, Y., Sparks, D.L. (2001) ATR- FTIR Spectroscopic Investigation on Phosphate Adsorption Mechanisms at the Ferrihydrite- Water Interface. Journal of Colloid and Interface Science 241 (2), 317–326.

Bastin, O., Janssens, F., Dufey, J., Peeters, A. (1999) Phosphorus removal by a synthetic iron oxide– gypsum compound, Ecological Engineering, 12:339-51. 61.

Bautista, M.C., Bomati-Miguel O., del Puerto M.M., Serna, C.J., Veintemillas-Verdaguer, S. (2005) Surface characterisation of dextran-coated iron oxide nanoparticles prepared by laser pyrolysis and coprecipitation, J. Magn. Magn. Mater. 293, 20–27.

Bentov, S., Aflalo, E.D., Tynyakov, J., Glazer, L., Sagi, A. (2016) Calcium phosphate mineralization is widely applied in crustacean mandibles. Scientific Report 6:22118.

Biswas, B.K., Inoue K., Ghimire, K.N., et. al. (2007) The adsorption of phosphate from an aquatic environment using metal-loaded orange waste, Department of Applied Chemistry, Saga University, Honjo 1, Saga 840:8502.

Bowker, R.P.G:, Stensel, H.D. (1990) Phosphorus Removal from Wastewater, 1st Edition, Pollution technology review ; no. 189. New Jersey, USA.

Boyer, C., Whittaker, M.R., Bulmus, V., Liu, J., Davis, T.P. (2010) The design and utility of polymerstabilized iron-oxide nanoparticles for nanomedicine applications, NPG Asia Mater. 2(1), 23-30.

Cao, Y., Bai, G., Chen, J., Tian, W., Wang, S., Yang, W. (2006) Chromatogr. B 833 236–244.

Carpenter, R.S., Caraco, N.F., Corell, D.L., Howart, R.W. (1998) Non-point pollution of surface waters with phosphorus and nitrogen, Ecological Applications 8(3).

Carpenter, S.R., Caraco, N.F., Correll, D.L., Howarth, R.W., Sharpley, A.N., Smith, V.H. (1998) Nonpoint pollution of surface waters with phosphorus and nitrogen. Ecol. Appl. 8, 559–568.

Chen, B., Chen, Z., Lv, S. (2011) A novel magnetic biochar efficiently sorbs organic pollutants and phosphate, Bioresource Technology, 102 (2011) 716–723.

Chen, B., Zhou, D., Zhu, L. (2008) Transitional adsorption and partition of nonpolar and polar aromatic contaminants by biochars of pine needles with different pyrolytic temperatures. Environ. Sci. Technol. 42, 5137–5143.

Chitrakar, R., Tezuka, S., Sonoda, A., Sakane, K., Ooi, K., Hirotsu, T. (2006) Phosphate adsorption on synthetic goethite and a kaganeite, Journal of Colloid and Interface Science, 298-602.

Chitrakar, R., Tezuka, S., Sonoda, A., Sakane, K., Ooi, K., Hirotsu, T. (2006) Phosphate adsorption on synthetic goethite and akaganeite. Journal of Colloid and Interface Science 298 (2), 602–608.

Choi, S. (2016) Phosphorus removal using titanium dioxide nanoparticles in wastewater treatment, Master Thesis,Wilfrid Laurier University, Waterloo, Ontario, Canada, 14-19.

Comba, S., Molfetta A., Sethi R. (2011) A comparison between field applications of nano, micro-, and millimetre c zero-valent iron for the remediation of contaminated aquifers, Water, Air, and Soil Pollution, 215, 595–607,

Cordell D., Drangert J.O., White S. (2019) The story of phosphorus: Global food security and food for thought, Global Environmental Change 19, 292-305

Cordell, D., Rosemarin, A., Schr€oder, J.J., Smit, A.L. (2011) Towards global phosphorus security: a systems framework for phosphorus recovery and reuse options, Chemosphere 84, 747-758.

Cornell, R.M., Schwertmann, U. (2000) Iron oxides in the laboratory: Preparation and characterization, Wiley, Weinheim, 188.

Cushing, B.L., Kolesnichenko, V.L., O'Connor, C.J., (2004) Chemical Reviews, 104 (9), 3893-3946.

Daou, T.J., Begin-Colin, S., Grenčche, J.M., Thomas, F., Legaré, P., Pourroy, G. (2007) Phosphate adsorption properties of magnetite-based nanoparticles, Chemistry of Materials, 19, 4505-4994.

Davila-Jimenez, M.M., Elizalde-Gonzalez, M.P., Pelaez-Cid, A.A. (2005) Adsorption interaction between natural adsorbents and textile dyes in aqueous solution, Colloids and Surface A Physicochemical and Engineering Aspects, 254, 107-114.

de Vicente, I., Merino-Martos, A., Cruz-Pizarro, L., de Vicente, J. (2010) On the use of magnetic nano and microparticles for lake restoration, Journal of Hazardous Materials 181., 375-381.

de-Bashan, L.E., Bashan, Y., (2004) Recent advances in removing phosphorus from wastewater and its future use as fertilizer (1997e2003). Water Research, 38, 422-4246.

Dryden, F.D., Stern, G. (1968) Renovated waste water creates recreational lake, Environmental Science Technology, 2., 268-278.

Elzinga, E.J., Sparks, D.L. (2007) Phosphate adsorption onto hematite: an in situ ATR-FTIR investigation of the effects of pH and loading level on the mode of phosphate surface complexation. Journal of Colloid and Interface Science 308 (1), 53–70.

Farber, E. (1966) History of Phosphorus, Publications of the United States National Museum, Washingon D. C., USA.

Fatima, H., Kyo-Seon, K. (2018) Iron-based magnetic nanoparticles for magnetic resonance imaging, Advanced Powder Technology 29, 2678–2685.

Franco, D., Lee, J., Arbelaeza, S., Cohen, N., Kim, J-Y.(2017) Removal of phosphate from surface and wastewater via electro coagulation, Ecological engineering, 108, 589-596.

Freundlich, H. (1907) Über die adsorption in lösungen, Zeischrift für Phys. Chemie 57, 385-470.

Gao, S., Wang, C., Pei, Y. (2013) Comparison of different phosphate species adsorption by ferric and alum water treatment residuals, Journal of Environmental Sciences. 25:986-92. 52.

Geelhoed, J.S., Hiemstra, T., Van Riemsdijk, W.H. (1997) Phosphate and sulfate adsorption on goethite: Single anion and competitive adsorption, Geochimica et Cosmochimica Acta., 61:2389-96.

Genz, A., Kornmüller, A., Jekel, M. (2004) Advanced phosphorus removal from membrane filtrates by adsorption on activated aluminium oxide and granulated ferric hydroxide, Water Research, 38:3523-30. 40.

Giang, T., Le, T., Paiboon S. (2015) Magnetic Particles for Phosphorus Adsorption in Simulated Phosphate Solution, 4th International Conference on Informatics, Environment, Energy and Applications, Volume 82 of IPCBEE, Thailand.

Glimcher, M. J. (2006) Bone: Nature of the calcium phosphate crystals and cellular, structural, and physical chemical mechanisms in their formation, Reviews in Mineralogy and Geochemistry 64(1), 223-282.

Gruère, G.P., Narrod, C.A., Abbott, L. (2011) Agricultural, food, and water nanotechnologies for the poor: opportunities, constraints, and the role of the consultative group on International Agricultural Research, International Food Policy Research Institute.

Guaya, D., Valderrama, C., Farran, A., Armijos, C., Cortina, J. L. (2015) Simultaneous phosphate and ammonium removal from aqueous solution by a hydrated aluminum ox-

ide modified natural zeolite Chemical Engineering Journal, 271:204-13. 53.

Hacıosmanoğlu, G.G., (2019) Adsorption of endocrine disrupting compounds by magnetic nanoparticles, PhD Thesis, Marmara University, Istanbul, Turkey, 21-76.

Havukainen, J., Nguyen, M.T., Hermann, L., Horttanainen, M., Mikkila, M., Deviatkin, I., Linnanen, L. (2016) Potential of phosphorus recovery from sewage sludge and manure ash by thermochemical treatment, Waste Management, 49, 221-229.

Horikoshi, S., Serpone, N. (2013) Introduction to Nanoparticles in Microwaves in Nanoparticle Synthesis, Wiley-VCH Verlag GmbH& Co. KGaA, 1-24.

Jeongyun, C., Jinwook, C., Wonhee, L., Han-Su, L., Jong-Oh, K. (2016) Recovery of Phosphate by Magnetic Iron Oxide Particles and Iron Oxide Nanotubes in Water, Water, Air, Soil Pollution, 227-131.

Jiang, D., Amano, Y., Machida, M. (2017) Removal and recovery of phosphate from water by a magnetic Fe_3O_4@ASC adsorbent, Journal of Environmental Chemical Engineering 5, 4229-4238.

Johansson, K., Perzon, M., Fröling, M., Mossakowska, A., Svanström, M. (2008) Sewage sludge handling with phosphorus utilization – life cycle assessment of four alternatives. J. Clean. Prod. 16, 135–151.

Juhászné, Sz. A., Dojcsákné, K. T. E. (2012) A nanomeretű szuperparamágneses vasoxid részecskék előállítási lehetőségei, Egészségtudományi Közlemények, 2. kötet, 1. szám, 95-98.

Jung, K.W., Jeong, T.U., Hwang, M.J., Kim, K., Ahn, K.H. (2015) Phosphate adsorption ability of biochar/Mg-Al assembled nanocomposites prepared by aluminum-electrode based electro-assisted modification method with MgCl2 as electrolyte. Bioresour. Technol. 198, 603–610.

Kabayama, M., Kawasaki, N., Nakamura, T., Sakiyama, T., Araki, M., Tanada, S. (2003) Characteristics of Phosphate Ion Adsorption–Desorption onto Aluminum Oxide Hydroxide for Preventing Eutrophication, Journal of Chemical Engineering of Japan,

36:499-505.

Kabayama, M., Kawasaki, N., Nakamura, T., Tanada, S. (2005) Adsorption/Desorption Characteristics of Phosphate Ion onto Calcined Boehmite Surface, e-Journal of Surface Science and Nanotechnology, 3:63-9.

Kölbel, B. (2007) Nanocomposites Composite Materials, 2, 14–18.

Kósa, I., Pósfai, M. (2007) Hidrológiai Közlöny, 87, 90-92.

Lai, L., Xie, Q., Chi, L., Gu, W., Wu, D. (2016) Adsorption of phosphate from water by easily separable Fe_3O_4@SiO_2 core/shell magnetic nanoparticles functionalized with hydrous lanthanum oxide, Journal of Colloid and Interface Science 465, 76–82.

Lakshmanan, R., Okoli, C., Boutonnet, M., Järås, S., Rajarao. G. K. (2014) Microemulsion prepared magnetic nanoparticles for phosphate removal: Time efficient studies, Journal of Environmental Chemical Engineering, 2:185-9.

Lalley, J., Han, C., Li, X., Sionysiou, D., Nadagouda, M. (2016) Phosphate adsorption using modified iron oxide-based sorbents in lake water: Kinetics, equilibrium, and column tests, Chemical Engineering Journal 284, 1386-1396.

Langmuir, I., (1918) The adsorption of gases on plane surfaces of glass, mica and platinum, Journal of the American Chemical Society, 40, 1361-1403.

Li, R., Yin, J., Wang, W., Li, Y., Zhang, Z. (2014) Transformation of phosphorus during drying and roasting sewage sludge. Waste Management, 34(7), 1211-1216.

Li, R.H., Wang, J.J., Zhou, B.Y., Awasthi, M.K., Ali, A., Zhang, Z.Q., Gaston, L.A., Lahori, A.H., Mahar, A. (2016a) Enhancing phosphate adsorption by Mg/Al layered double hydroxide functionalized biochar with different Mg/Al ratios. Sci. Total Environ. 559, 121–129.

Li, R.H., Wang, J.J., Zhou, B.Y., Awasthi, M.K., Ali, A., Zhang, Z.Q., Lahori, A.H., Mahar, A. (2016b) Recovery of phosphate from aqueous solution by magnesium oxide

decorated magnetic biochar and its potential as phosphate-based fertilizer substitute. Bioresour. Technol. 215, 209–214.

Lin, Y-F., Chen, H-W., Chen, Y-C., Chiou, C-S. (2013) Application of magnetite modified with polyacrylamide to adsorb phosphate in aqueous solution, Journal of the Taiwan Institute of Chemical Engineers, 44:45-51.

Loganathan, P., Vigneswaran, S., Kandasamy, J., Bolan, N. S. (2014) Removal and recovery of phosphate from water using sorption, Critical Reviews in Environmental Science and Technology, 44 (8), 847-907.

Lueng, C., Brigante, M., Antelo, J., Avena, M. (2006) Kinetics of phosphate adsorption on goethite: Comparing batch adsorption and ATR-IR measurements, Journal of Colloid and Interface Science, 300-511.

Maciel, J.C., Andrad, P.L., Neri, D.F.M., Carvalho Jr, L.B., Cardoso, C.A., Calazans, G.M.T., Aguiar, J.A., Silva, M.P.C. (2012) Preparation and characterization of magnetic levanparticles as matrix for trypsin immobilization. J. Magn. Magn. Mater.324, 1312–1316.

Majidnia, Z., Idris, A. (2015) Evaluation of cesium removal from radioactive waste water usnig maghemite PVA-alginate beads, Chemical Engineering Journal 262, 372- 382

Mandel, K., Derenkova-Tuhtan, A., Hutter, F., Gellermann, C., Steinmetz, H., Sext, G., (2013) Layered double hydroxide ion exchangers on superparamagnetic microparticles for recovery of phosphate from waste water, Journal of Materials Chemisrty A, 1840-1848.

Markeb, A. A.; Alonso, A., Dorado, A., Sánchez, A., Font, X. (2016) Phosphate removal and recovery from water using nanocomposite of immobilized magnetite nanoparticles on cationic polymer, Environmental Technology.

Markeb, A. M. A. A. (2017) Environmental Applications of Engineered Nanomaterials: Sythesis and Characterization, PhD Thesis, Universitat Autonóma de Barcelona, Barcelona, Spain, 12-110.

Miot, J., Benzerara, K., Morin, G., Bernard, S., Beyssac, O., Larquet, E., Kappler, A., Guyot, F. (2009) Transformation of vivianite by anaerobic nitrate-reducing iron-oxidizing bacteria. Geobiology 7 (3), 373–384.

Mueller, N. C., Braun, J., Bruns, J., Cernık, M., Rissing, P., Rickerby, D., Nowack, B. (2012) Application of nanoscale zero valent iron (NZVI) for groundwater remediation in Europe, Environmental Science and Pollution Research 19, 550-558.

Nguyen, T.A.H., Ngo, H.H., Guo, W.S., Zhang, J., Liang, S., Lee, D.J., Nguyen, P.D., Bui, X.T. (2014) Modification of agricultural waste/by-products for enhanced phosphate removal and recovery: potential and obstacles. Bioresour. Technol. 169, 750–762.

Oliveira, M., Ribeiro, D., Nobrega, J. M., Machado, A. V., Brito, A. G., Nogueira, R. (2011) Removal of phosphorus from water using active barriers: Al_2O_3 immobilized on to polyolefins, Environmental Technology,32:989-95.

Onyango, M.S., Kuchar, D., Kubota, M., Matsuda, H. (2007) Adsorptive removal of phosphate ions from aqueous solution using synthetic zeolite. Industrial Engineering and Chemistry Research, 46, 894–900.

Pan, G., Li, L., Zhao, D., Chen, H., (2010) Immobilization of non-point phosphorus using stabilized magnetite nanoparticles with enhanced transportability and reactivity in soils, Environmetal Pollution, 158., 35-40.

Parfitt, R.L., Atkinson, R.J. (1976) Phosphate adsorption on goethite (α-FeOOOH). Nature 264 (5588), 740–742.

Persson, P., Nilsson, N., Sjöberg, S. (1996) Structure and Bonding of Orthophosphate Ions at the Iron Oxide-Aqueous Interface. Journal of Colloid and Interface Science 177 (1), 263–275.

Ramsden, J.J. (2013) The nanotechnology industry, Nanotechnology Perceptions Vol. 9, UK.

Russel, J.D., Parfitt, R.L., Frasser, A.R., Farmer, V.C. (1974) Surface structures of gibbsite goethite and phosphated goethite. Nature 248 (5445), 220–221.

Salah, A., Jozwiak, P., Zaghib, K., Garbarczyk, J., Gendron, F., Mauger, A., Julien C.M. (2006) Spectrochim. Acta, Part A: Molec. Biomolec. Spectrosc., 65, 1007.

Sarıbuğa, S. (2014) Manyetik nanopartikullerin analiktik incelenmesi Master Thesis, Istanbul Teknik University, Istanbul, Turkey.

Sawyer, C.N., McCarty P.L., Parkin, G.F. (1994) Chemistry for Environmental Engineering, 4th Edition, Civil Engineering Series, Singapore, Malaysia.

Scherrer, P. (1918) Bestimmung der Grosse und der InnerenStruktur von KolloidteilchenMittelsRontgenstrahlen, Nachrichten von der Gesellschaft der Wissenschaften, Gottingen, Mathematisch-PhysikalischeKlasse, 2, 98-100.

Seo-Young, Y., Lee, C. G., Park, J. A., Kim, J. H., Kim, S. B., Lee, S-H., Choi, J. W. (2014) Kinetic, equilibrium and thermodynamic studies for phosphate adsorption to magnetic iron oxide nanoparticles, Chemical Engineering Journal Volume 236, 341-347.

Shin, W. K., Cho, J., Kannan, A. G., Lee, Y-S., Kim, D.W. (2016) Cross-linked composite gel polymer electrolyte using mesoporous methacrylate-functionalized SiO_2nanoparticles for lithium-ion polymer batteries, Scientific Reports, 6, 26332.

Sips, R., (1948) The Structure of a Catalyst Surface, The Journal of Chemical Physics, 16, 490-495.

Srivastava, S., Agrawal, S. B., Mondal, M. K. (2015) Environmental Science Pollution-Res.,22, 15386 -15415.

Su, C., Puls, R. W., Krug, T. A., Watling, M. T., O'Hara, S. K., Quinn, J. W., Ruiz, N. E. (2012) A two and half-year-performance evaluation of a field test on treatment of source zone tetrachloro ethene and its chlorinated daughter products using emulsified zero valent iron nanoparticles, Water Research 46, 5071-5084.

Su, Y., Yang, W., Sun, W., Li, Q., Shang, J. K. (2015) Synthesis of mesoporous cerium–zirconium binary oxide nanoadsorbents by a solvo thermal process and their effective adsorption of phosphate from water, Chemical Engineering Journal, 268:270-9.

Suciu, N.A., Lamastra, L., Trevisan, M., (2015) PAHs content of sewage sludge in Europe and its use as soil fertilizer, Waste Manag., 41, 119-127.

Sun, Z.X., Su, F.W., Forsling, W., Samskog, P.O. (1998) Surface Characteristics of Magnetite in Aqueous Suspension, Journal of Colloid and Interface Science 197, 151-159.

Szittya, O. (1999) Digitálisés Analóg Technika. LSI Oktató központ

Tang, J., Chen. J., Huang, W., Li, D., Zhu, Y., Tong, Y., Zhang, Y. (2014) Porous $Pr(OH)_3$ nanowires as novel high-performance adsorbents for phosphate removal, Chemical Engineering Journal, 252-202-9.

Tarayre, C., De Clercq, L., Charlier, R., Michels, E., Meers, E., Camargo-Valero, M., Delvigne, F., (2016) New perspectives for the design of sustainable bioprocesses for phosphorus recovery from waste, Bioresource Technology, 206:264-274.

Thorek, D. L J., Chen, A. K., Czupryna, J., Tsourkas, A. (2006) Superparamagnetic Iron Oxide Nanoparticle Probes for Molecular Imaging, Annals of Biomedical Engineering, 34 (1), 23-38.

Towler, P. H., Smith, J.D., Dixon, D.R. (1996) Anal. Chim. Acta 328, 53–59.

Toy, A.D.F., (1973) The Chemistry of Phosphorus, 1st Edition, Pergamon Texts in Inorganic Chemistry, Volume 3, Washingon D. C., USA.

Tu, Y.J., You, C.F. (2014) Phosphorus adsorption onto green synthesized nano bimetal ferrites: equilibrium, kinetic and thermodynamic investigation, Chemical Engineering Journal, 251, 285-292.

Urano, K., Tachikawa, H. (1991) Process development for removal and recovery of phosphorus from wastewater by a new adsorbent. 1. Preparation method and adsorption capability of a new adsorbent. Industrial Engineering and Chemistry Research, 30, 1893–1896.

Wasay, S. A., Tokunaga, S., Park, S. W. (1996) Removal of Hazardous Anions from

Aqueous Solutions by La(lll)- and Y(lll)-lmpregnated Alumina, Separation Science and Technology, 31:1501-14.

Welles, L. (2018) Enhanced Biological Phosphorus Removal: Metabolic Insights and Salinity Effects, 1st Edition., CRC Press, London, United Kingdom.

Westheimer, F. H. (1987) Why nature chose phosphates, Science 235, 1173.

Wu, B., Fang, L., Fortner, J. D., Guan, X., Lo, I. M. (2017) Highly efficient and selective phosphate removal from wastewater by magnetically recoverable $La(OH)_3/Fe_3O_4$ nanocomposites, Water Research, 126, 179-188.

Wu, D., Shen, Y., Ding, A., Qiu, M., Yang, Q., Zheng, S. (2013) Phosphate removal from aqueous solutions by nanoscale zero-valent iron, Environmental Technology, 34:2663-9.

Xie, C., Zhao, J., Tang, J., Xu, J., Lin, X., Xu, X. (2010) The phosphorus fractions and alkaline phosphatase activities in sludge, Bioresource Technology, 102, 2455-2461.

Xu, N., Li, Y., Zheng, L., Gao, Y., Yin, H., Zhao, J., Chen, Z., Chen, J., Chen, M. (2014) Synthesis and application of magnesium amorphous calcium carbonate for removal of high concentration of phosphate, Chemical Engineering Journal, 251:102-10.

Xu, X., Zhao, Y., Sima, J., Zhao, L., Masek, O., Cao, X. (2017) Indispensable role of biochar-inherent mineral constituents in its environmental applications: a review. Bioresour. Technol. 241, 887-899.

Yavuz, C.T., Prakash, A., Mayo, J.T., Colvin, V.L. (2009) Magnetic separations: From steel plants to biotechnology, Chemical Engineering Science, 64, 2510-2521.

Yuchi, A. (2014) Diverse secondary interactions between ions exchanged into the resin phase and their analytical application, Analitycal Sciences, 30, 51-57.

Zach-Maor, A., Semiat, R., Shemer, H. (2011a) Adsorption desorption mechanism of phosphate by immobilized nanosized magnetite layer: interface and bulk interactions, Journal of Colloid and Interface Science, 363, 608-614.

Zach-Maor, A., Semiat, R., Shemer, H. (2011b) Synthesis, performance, and modeling of immobilized nano-sized magnetite layer for phosphate removal, Journal of Colloid and Interface Science, 357-440-6.

Zeng, L., Li, X., Liu, J. (2004) Adsorptive removal of phosphate from aqueous solutions using iron oxide tailings, Water Research, 38:1318-26.

Zhang, L., Gao, Y., Li, M., Liu, J. (2015) Expanded graphite loaded with lanthanum oxide used as a novel adsorbent for phosphate removal from water: performance and mechanism study, Environmental Technology, 36:1016-25.

Zhou, K., Barjenbruch, M., Kabbe, C., Inial, G., Remy, C. (2016) Phosphorus recovery from municipal and fertilizer wastewater: China's potential and perspective, Journal of Environmental Sciences, 52:151-159

Zhu, Z., Zeng, H., Zhu, Y., Yang, F., Zhu, H., Qin, H., Wei, W. (2013) Kinetics and thermodynamic study of phosphate adsorption on the porous biomorph-genetic composite of α-Fe2O3/Fe3O4/C with eucalyptus wood microstructure, Separation and Purification Technology, 117:124-30.

Zong, E., Wei, D., Wan, H., Zheng, S., Xu, Z., Zhu, D. (2013) Adsorptive removal of phosphate ions from aqueous solution using zirconia-functionalized graphite oxide, Chemical Engineering Journal, 221:193-203.

ÖZGEÇMİŞ

Informations:

+36309387797

+905522081340
gulyasanett93@gmail.com
I.sz. ltp. street 16.
Eger, 3300
Hungary

As a Certified Master in Applied Environmental Studies, I intend to use my extensive knowledge gained in the Hungarian and international environment. In the recent years I have acquired new and modern analytical techniques and approach that I am ready to introduce to my future employer.

LIST OF RELEVANT EXPERIENCES

- October, 2018 – October, 2019: Phosphate recovery from sewage sludge supernatants using magnetic nanoparticles (Thesis work – laboratory experiments) – Istanbul, Turkey
- September, 2015 – January, 2016: Chemical properties and usage of the thermal waters of the Eger region (Thesis work – laboratory experiments) – Szeged, Hungary
- July - August, 2015: Learning about the process of water extraction and wastewater treatment (Summer Internship) – Heves Megyei Vízmű ZRT., Eger, Hungary

STUDIES

October, 2016 – October, 2019 Marmara Üniversitesi, Istanbul

Environmental Studies - Certified Master in Applied Environmental Studies (MSc)

- Turkish language scholarship program - YTB Türkiye Burslari
- Research-relevant course: Environmental Chemistry
- Independent and group work during laboratory tests
- Results:
    - Thesis (2018 – 2019)

September, 2011 – January, 2016 University of Szeged

Environmental Studies - Expert in Applied Environmental Studies (BSc)

- Specialization: waste treatment and disposal
- Research-relevant courses: Environmental protection technologies laboratory, Analytical chemistry laboratory, Hydrogeology

YOUTH WORK

- November, 2015: Mobility of Youth Workers – Erasmus+ project: Gloucestershire, UK
- 2013 – 2015: President of ESN Szeged (Erasmus Student Network), (coordinating 10 people)
    - AGM (Annual General Meeting) Ankara (2015), AGM Milano (2014), NPs (National Platform): Győr, Pécs, Debrecen, Gödöllő

LANGUAGES

- Hungarian - Native or bilingual proficiency
- English - Professional working proficiency
- Turkish - Elementary proficiency

INSTRUMENTS/ COMPUTER PROGRAMMES

- Spectrophotometer, Photoelectron flame photometer, Zeta-meter
- Microsoft MS Office: Excel (spreadsheet, diagram editing, functions)

INTERESTS

Psychological and scientific books, magazines; gardening; baking; swimming

OTHER

- Thesis: Phosphate recovery from sewage sludge supernatants using magnetic nanoparticles, (Doc. Dr. Neslihan Semerci)
- Thesis: Chemical properties and usage of the thermal waters of the Eger region (dr. István Hannus professor emeritus, dr. János Halász †)

Driving license: ’B’ category